Available on CMS information server

CMS NOTE RN 2003-002

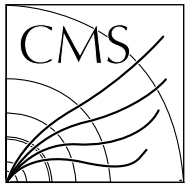

The Compact Muon Solenoid Experiment

CMS Note

Mailing address: CMS CERN, CH-1211 GENEVA 23, Switzerland

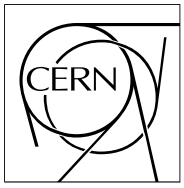

July 4, 2003

Squark and gluino reconstruction with the CMS detector

M. Chiorboli, A. Tricomi

Dipartimento di Fisica e Astronomia dell'Università di Catania
and INFN Sezione di Catania,
Via Santa Sofia 64, Catania (Italy)

Abstract

The capability of the CMS detector to reconstruct squarks and gluino is investigated. A method to reconstruct sbottom, light squark and gluino mass peaks has been developed and applied in three different mSUGRA scenarios. With favourable parameters, a resolution better than 10% can be achieved for all the reconstructed sparticles already with 10 fb^{-1} of integrated luminosity, under the assumption of a known $\mathrm{M}(\tilde{\chi}_1^0)$.

1 Introduction

Several studies have been performed up to now by the CMS Collaboration to evaluate the detector capability to observe an excess of Supersymmetric events over the Standard Model ones. It has been found that for an integrated luminosity of 300 fb^{-1} squarks and gluinos could be observed up to a mass of 2 TeV [1]. Of course, this is not the end of the game: the "excess" over the Standard Model alone is not the proof of Supersymmetry existence. It is reasonable to demand stronger evidence: if new particles are observed, it is necessary to measure, in a second stage, their masses and their couplings to Standard Model particles and to other sparticles. Eventually, with a deep knowledge of the spectrum of the observed particles, it could be desirable to extrapolate the model parameters from the measured quantities. The very final goal of the next-generation detectors should be to give a complete view of the supersymmetry model such as LEP and TeVatron have done with the Standard Model.

Such kind of *spectroscopic* studies on supersymmetry have never been performed by the CMS collaboration. In this paper a work done to evaluate the detector capability to reconstruct squarks and gluinos and to observe their mass peaks is presented. This kind of analysis is based on a different approach with respect to the ones used in previous studies: the aim is not the definition of some parameter regions of observability. A particular pattern of the supersymmetric spectrum has to be considered: the detector capability to operate the reconstructions is hence evaluated in that scenario. To do this, three points in the mSUGRA parameter space have been chosen among the ones suggested in the Ref. [2] and each of them has been accurately analysed.

The decay chains under examination are $\tilde{\mathrm{g}} \to \tilde{\mathrm{b}}\mathrm{b} \to \tilde{\chi}_2^0\mathrm{b}\mathrm{b} \to \tilde{\ell}_{\mathrm{R}}^{\pm}\ell^{\mp}\mathrm{b}\mathrm{b} \to \tilde{\chi}_1^0\ell^{\pm}\ell^{\mp}\mathrm{b}\mathrm{b}$ and $\tilde{\mathrm{g}} \to \tilde{\mathrm{q}}\mathrm{q} \to \tilde{\chi}_2^0\mathrm{q}\mathrm{q} \to \tilde{\ell}_{\mathrm{R}}^{\pm}\ell^{\mp}\mathrm{q}\mathrm{q} \to \tilde{\chi}_1^0\ell^{\pm}\ell^{\mp}\mathrm{q}\mathrm{q}$; the aim is the reconstruction of gluinos, sbottoms (in the rest of the note *squark* indicates a supersymmetric partner of a light quark, while the third generation squarks are explicitly called *stops* and *sbottoms*). In both cases, the reconstruction are performed starting from the $\tilde{\chi}_2^0 \to \ell^+\ell^-\tilde{\chi}_1^0$ decay, with $\ell = \mathrm{e}, \mu$. The branching ratios of these decays are strongly dependent on the $\tan\beta$ parameter, leading to a larger $\tilde{\chi}_2^0 \to \tau^+\tau^-\tilde{\chi}_1^0$ branching ratio, and to a smaller $\tilde{\chi}_2^0 \to \ell^+\ell^-\tilde{\chi}_1^0$ one with increasing $\tan\beta$. This effect is of fundamental importance for the desired reconstruction: three points with different $\tan\beta$ values out of the 13 proposed have been chosen. All of them were selected among the points with relatively low values of m_0 and $m_{1/2}$ in order to have low mass spectrum and hence a high production cross section for squarks and gluinos and possibly allowing early observation.

The selected points are defined as follows:

Point B: $m_0 = 100$ GeV/c^2, $m_{1/2} = 250$ GeV/c^2, $\tan\beta = 10$, $\mathrm{A}_0 = 0$, and $\mu > 0$;

Point G: $m_0 = 120$ GeV/c^2, $m_{1/2} = 375$ GeV/c^2, $\tan\beta = 20$, $\mathrm{A}_0 = 0$, and $\mu > 0$;

Point I: $m_0 = 180$ GeV/c^2, $m_{1/2} = 350$ GeV/c^2, $\tan\beta = 35$, $\mathrm{A}_0 = 0$, and $\mu > 0$.

Table 1 summarizes the supersymmetric particle masses as given at Point B, G and I with the procedure described above. The decay branching ratios in all the scenarios have been evaluated using the release `ISASUGRA 7.51` [3]. The mSUGRA parameters have been given as input to the `ISASUGRA 7.51` code, which executes the running-down of the RGE's to the electroweak scale. The low-scale MSSM parameters extracted by `ISASUGRA` have been given to `PYTHIA 6.152` [4] for the generation of the events. `CMSJET 4.801` [5] has been used for the detector simulation.

2 Sbottom reconstruction at Point B

The five mSUGRA parameters for point B given as input to `ISASUGRA 7.51` are

$$\begin{aligned} m_0 &= 100 \text{ GeV/c}^2 \\ m_{1/2} &= 250 \text{ GeV/c}^2 \\ \tan\beta &= 10 \\ A_0 &= 0 \\ \mu &> 0 \end{aligned}$$

The SUSY processes produced by the `PYTHIA 6.152` generator in 14 TeV proton-proton collisions are shown in Table 2, together with their production cross section. The dominant contributions are from squark-gluino, gluino-gluino and squark-squark production. The total production cross section of supersymmetric events is 57.77 pb.

Table 1: Spectra at point B, G and I as given by PYTHIA 6.152 with input parameters taken from ISASUGRA 7.51.

Particle	Mass (GeV/c^2)		
	Point B	Point G	Point I
$\tilde{u}_L$	536.965	773.878	738.361
$\tilde{d}_L$	542.823	778.015	742.711
$\tilde{c}_L$	536.965	773.878	738.361
$\tilde{s}_L$	542.823	778.015	742.711
$\tilde{t}_1$	392.938	587.234	555.355
$\tilde{b}_1$	495.996	701.947	640.321
$\tilde{u}_R$	519.129	747.945	714.924
$\tilde{d}_R$	520.884	745.804	713.165
$\tilde{c}_R$	519.129	747.945	714.924
$\tilde{s}_R$	520.884	745.804	713.165
$\tilde{t}_2$	575.910	778.566	736.020
$\tilde{b}_2$	523.966	748.385	713.294
$\tilde{e}_R$	136.180	183.170	221.330
$\tilde{\mu}_R$	136.180	183.170	221.330
$\tilde{\tau}_2$	200.316	285.431	304.794
$\tilde{e}_L$	196.580	278.880	295.690
$\tilde{\nu}_{e_L}$	179.774	267.120	284.588
$\tilde{\mu}_L$	196.580	278.880	295.690
$\tilde{\nu}_{\mu_L}$	179.774	267.120	284.588
$\tilde{\tau}_1$	127.569	154.062	143.683
$\tilde{\nu}_{\tau_L}$	179.052	263.402	271.171
$\tilde{g}$	595.070	860.820	809.810
$\tilde{\chi}_1^0$	95.623	150.020	139.793
$\tilde{\chi}_2^0$	174.745	277.121	257.860
$\tilde{\chi}_1^\pm$	173.835	276.794	257.555
$\tilde{\chi}_3^0$	339.890	477.932	446.690
$\tilde{\chi}_4^0$	361.051	493.561	462.227
$\tilde{\chi}_2^\pm$	361.628	494.327	463.336

Table 2: Production cross sections for the SUSY process in proton-proton collisions at $\sqrt{s} = 14$ TeV, as given by PYTHIA 6.152 with input parameters taken from ISASUGRA. The symbol $\tilde{\chi}$ indicates charginos and neutralinos, while $\tilde{q}$ is used only for the first two generation squarks. Sbottoms and stops are represented separately from the other squarks.

Process	σ (pb)
$\tilde{g}\tilde{g}$	6.99
$\tilde{\ell}\tilde{\ell}$	0.54
$\tilde{\chi}\tilde{\chi}$	1.90
$\tilde{\chi}\tilde{g}$	0.48
$\tilde{\chi}\tilde{q}$	1.89
$\tilde{q}\tilde{g}$	28.31
$\tilde{q}\tilde{q}$	14.16
$\tilde{q}\tilde{b}$	0.36
$\tilde{b}\tilde{b}$	0.52
$\tilde{b}\tilde{g}$	0.71
$\tilde{t}\tilde{t}$	1.83
Total	57.77

Detailed tables for the branching ratios of the main decays at point B can be found in Ref. [6]. It is interesting to notice that the gluino can decay into sbottoms with quite large branching ratio and that $\tilde{\chi}_2^0$ cannot decay into $\tilde{\ell}_L$: its main leptonic decay channel is $\tilde{\chi}_2^0 \to \tilde{\ell}_R \ell$, with $\tilde{\ell}_R$ decaying into $\tilde{\chi}_1^0 \ell$ with 100% branching ratio. The three body decay $\tilde{\chi}_2^0 \to \tilde{\chi}_1^0 \ell^+ \ell^-$ is also possible, but with 0.04% branching ratio, and so negligible compared to the two body decay.

The sbottom mass peak can be reconstructed exploiting the decay chain:

$$\begin{array}{rcl} \tilde{\mathrm{b}} & \rightarrow & \tilde{\chi}_2^0 \mathrm{b} \\ & & \downarrow \\ & & \tilde{\ell}_{\mathrm{R}}^{\pm} \ell^{\mp} \rightarrow \tilde{\chi}_1^0 \ell^{\pm} \ell^{\mp} \end{array} \tag{1}$$

where ℓ stands for e and μ; decays into taus are not considered. The first step of the reconstruction procedure is the identification of the $\tilde{\chi}_2^0$ from its decay products. Once $\tilde{\chi}_2^0$ has been reconstructed, it can be associated to a b to get the sbottom. Of course, the $\tilde{\chi}_1^0$ is undetectable, since it behaves like a heavy neutrino, and the final state $\tilde{\chi}_1^0 \ell^{\pm} \ell^{\mp}$ cannot be exactly determined. Nevertheless, due to the particular kinematic characteristics of the decay $\tilde{\chi}_2^0 \rightarrow \tilde{\ell}_{\mathrm{R}}^{\pm} \ell^{\mp} \rightarrow \tilde{\chi}_1^0 \ell^{\pm} \ell^{\mp}$ it is possible to perform the reconstruction of the $\tilde{\chi}_2^0$. It has infact already been demonstrated in past CMS studies [7] that, with favourable SUSY parameters, it will be possible to observe the typical edge in the distribution of the same flavour opposite sign lepton pairs [8]. The direct decay $\tilde{\chi}_2^0 \rightarrow \tilde{\chi}_1^0 \ell^+ \ell^-$ has a branching ratio of 0.04% at point B, negligible with respect to the branching ratio of the decay $\tilde{\chi}_2^0 \rightarrow \tilde{\ell}_{\mathrm{R}}^{\pm} \ell^{\mp} \rightarrow \tilde{\chi}_1^0 \ell^{\pm} \ell^{\mp}$, which is 16.44%. So, the end-point of the distribution will be given by the equation:

$$\mathrm{M}_{\ell^+\ell^-}^{\mathrm{max}} = \frac{\sqrt{\left(\mathrm{M}_{\tilde{\chi}_2^0}^2 - \mathrm{M}_{\tilde{\ell}}^2\right)\left(\mathrm{M}_{\tilde{\ell}}^2 - \mathrm{M}_{\tilde{\chi}_1^0}^2\right)}}{\mathrm{M}_{\tilde{\ell}}} \tag{2}$$

This end-point corresponds to the kinematic situation in which, in the $\tilde{\chi}_2^0$ rest frame, the two leptons are emitted back-to-back, as schematically illustrated in Fig. 1.

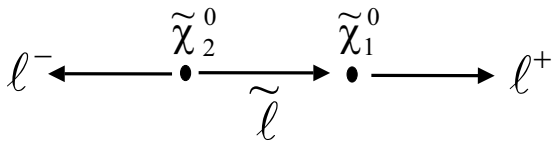

Figure 1: Schematic view of the decay $\tilde{\chi}_2^0 \rightarrow \tilde{\ell}_{\mathrm{R}}^{\pm} \ell^{\mp} \rightarrow \tilde{\chi}_1^0 \ell^{\pm} \ell^{\mp}$ at the end-point of the $\mathrm{M}_{\ell\ell}$ distribution.

The branching ratios for the entire decay chains are

$$\mathrm{BR}(\tilde{\mathrm{b}}_1 \rightarrow \tilde{\chi}_2^0 \mathrm{b} \rightarrow \tilde{\ell}_{\mathrm{R}}^{\pm} \ell^{\mp} \mathrm{b} \rightarrow \tilde{\chi}_1^0 \ell^{\pm} \ell^{\mp} \mathrm{b}) = 6.09\%, \tag{3a}$$

$$\mathrm{BR}(\tilde{\mathrm{b}}_2 \rightarrow \tilde{\chi}_2^0 \mathrm{b} \rightarrow \tilde{\ell}_{\mathrm{R}}^{\pm} \ell^{\mp} \mathrm{b} \rightarrow \tilde{\chi}_1^0 \ell^{\pm} \ell^{\mp} \mathrm{b}) = 4.12\%. \tag{3b}$$

The $\sigma \times$ BR's for the direct productions of sbottoms in proton-proton interactions can be calculated from these relations: they result 85.5 fb for $\tilde{\mathrm{b}}_1$ and 31.5 fb for $\tilde{\mathrm{b}}_2$.

To operate the sbottom reconstruction not only the sbottoms directly produced in proton-proton interactions have to be considered: sbottoms are abundantly produced also from gluino decays. It can be shown that:

$$\mathrm{BR}(\tilde{\mathrm{g}} \rightarrow \tilde{\mathrm{b}}_1 \mathrm{b} \rightarrow \tilde{\chi}_2^0 \mathrm{bb} \rightarrow \tilde{\ell}_{\mathrm{R}}^{\pm} \ell^{\mp} \mathrm{bb} \rightarrow \tilde{\chi}_1^0 \ell^{\pm} \ell^{\mp} \mathrm{bb}) = 1.05\% \tag{4a}$$

$$\mathrm{BR}(\tilde{\mathrm{g}} \rightarrow \tilde{\mathrm{b}}_2 \mathrm{b} \rightarrow \tilde{\chi}_2^0 \mathrm{bb} \rightarrow \tilde{\ell}_{\mathrm{R}}^{\pm} \ell^{\mp} \mathrm{bb} \rightarrow \tilde{\chi}_1^0 \ell^{\pm} \ell^{\mp} \mathrm{bb}) = 0.42\% \tag{4b}$$

and hence the $\sigma \times$ BR's for sbottoms coming from gluinos and then decaying into the whole decay chain are 449.9 fb and 179.7 fb for $\tilde{\mathrm{b}}_1$ and $\tilde{\mathrm{b}}_2$. In this case the sbottoms are more abundantly produced in gluino decays than in direct proton-proton collisions. The decay chain to be considered to perform sbottom reconstruction is hence:

$$\begin{array}{rcl} \tilde{\mathrm{g}} & \rightarrow & \tilde{\mathrm{b}} \mathrm{b} \\ & & \downarrow \\ & & \tilde{\chi}_2^0 \mathrm{b} \\ & & \downarrow \\ & & \tilde{\ell}_{\mathrm{R}}^{\pm} \ell^{\mp} \rightarrow \tilde{\chi}_1^0 \ell^{\pm} \ell^{\mp} \end{array} \tag{5}$$

A sketch of such a decay chain is shown in Fig. 2.

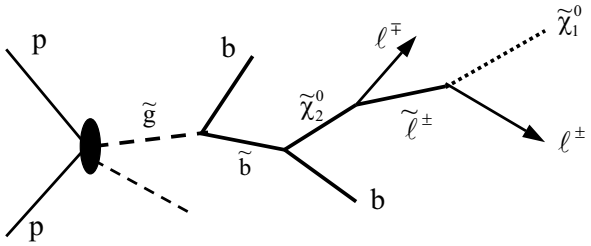

Figure 2: Pictorial view of the decay $\tilde{\mathrm{g}} \to \tilde{\mathrm{b}}_2\mathrm{b} \to \tilde{\chi}_2^0\mathrm{bb} \to \tilde{\ell}_{\mathrm{R}}^{\pm}\ell^{\mp}\mathrm{bb} \to \tilde{\chi}_1^0\ell^{\pm}\ell^{\mp}\mathrm{bb}$.

The probability of having two sbottoms decaying into the correct chain in an event is very small: 2.4 fb and 0.7 fb for $\tilde{\mathrm{b}}_1$ and $\tilde{\mathrm{b}}_2$ respectively, negligible compared to the single sbottom chain. In the rest of this paper events with only one gluino giving the decay chain (5) are considered. Such events are characterized by a final state with two high-p_{T} isolated leptons, two high-p_{T} b jets and missing energy resulting from the undetectable neutralino; the following selection criteria have therefore been applied to the generated SUSY events, handled by `CMSJET`:

- at least 2 same flavour opposite sign (SFOS) isolated leptons having $p_{\mathrm{T}} > 15$ GeV/c and $|\eta| < 2.4$, corresponding to the acceptance of the muon system. Only electrons and muons are considered in this study;
- at least 2 jets tagged as b jets, having $p_{\mathrm{T}} > 20$ GeV/c and $|\eta| < 2.4$.

Leptons are "isolated" if no charged particle tracks with $p_{\mathrm{T}} > 2$ GeV/c are present in a cone of $\Delta\mathrm{R} = 0.3$ in the tracker, and if no energy deposits above the threshold of 5 GeV are in a cone of $\Delta\mathrm{R} = 0.3$ around the lepton impact point on the calorimeter. In Table 3 for each SUSY generation process, the number of generated events and the number of events surviving each selection step of the procedure, are reported for an integrated luminosity of 10 fb^{-1}. No events survive among the directly produced slepton pairs neither chargino-neutralino pairs, since these events have no jets. Only a small amount of events are selected among the ones with direct production of squarks: these can survive because of a mistagging of the jets.

Table 3: Number of produced SUSY events. For each generation process, the number of events surviving the sequence of selection criteria for sbottom reconstruction, as described in the text, is shown.

	N ev in 10 fb^{-1}	2 leptons	2 b jets	2 SFOS isol. ℓ
$\tilde{\mathrm{b}}\tilde{\mathrm{b}}$	5153	2046	510	177
$\tilde{\mathrm{b}}\tilde{\mathrm{g}}$	7063	2219	643	163
$\tilde{\chi}\tilde{\chi}$	18999	2278	6	0
$\tilde{\chi}\tilde{\mathrm{g}}$	4767	865	92	22
$\tilde{\chi}\tilde{\mathrm{q}}$	18880	2683	20	6
$\tilde{\mathrm{g}}\tilde{\mathrm{g}}$	69943	14533	4242	872
$\tilde{\ell}\tilde{\ell}$	5378	1052	0	0
$\tilde{\mathrm{q}}\tilde{\mathrm{b}}$	3616	890	99	27
$\tilde{\mathrm{q}}\tilde{\mathrm{g}}$	283199	40309	5590	1394
$\tilde{\mathrm{q}}\tilde{\mathrm{q}}$	141609	12034	111	37
$\tilde{\mathrm{t}}\tilde{\mathrm{t}}$	18311	4819	1174	204
Total	576918	83728	12487	2902

Figure 3 shows the distribution of the same flavour opposite sign dilepton pairs for all the supersymmetric events passing the selection criteria. For events with more than one lepton pair, the two leptons closest in angle have been chosen, since studies performed at parton level show a small angular distance between the two leptons arising from $\tilde{\chi}_2^0$ [6]. The main contribution comes from the decay under study (solid histogram). Other non negligible contributions come from events in which both leptons arise from taus (dashed line), events in which at least one of the leptons comes from a W boson (dotted line); leptons from Z (dashed-dotted line), but this is a negligible channel. The first ones are produced mainly in $\tilde{\chi}_2^0 \to \tilde{\tau}_1\tau \to \tilde{\chi}_1^0\tau\tau$ decays, but others can come from charginos through the $\tilde{\chi}_1^{\pm} \to \tilde{\tau}_1\nu_{\tau}$ process; the second ones have different sources: W's coming from t-quarks given by the $\tilde{\mathrm{b}}_{1,2} \to \tilde{\chi}_1^{\pm}\mathrm{t}$ decay, W's produced in sbottom decays ($\tilde{\mathrm{b}}_{1,2} \to \tilde{\mathrm{t}}_1\mathrm{W}$), or W's coming from top produced in stop decay chains. The lower plot of the same figure represents the same distribution after a cut on the energy of the

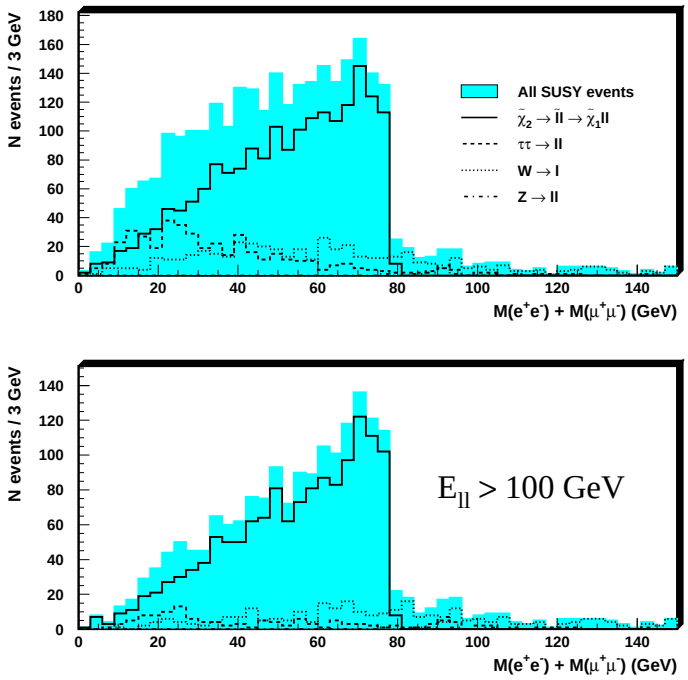

Figure 3: Invariant mass distribution of same flavour opposite sign isolated lepton pairs for the SUSY events passing the selection criteria described in the text. The shaded histogram refers to the whole SUSY sample. The individual contributions are separately shown: $\tilde{\chi}_2^0 \to \tilde{\ell}_{\rm R}^{\pm}\ell^{\mp} \to \tilde{\chi}_1^0\ell^{\pm}\ell^{\mp}$ (solid line), events with both leptons coming from taus (dashed line), events with at least one lepton coming from a W boson (dotted line), events with leptons coming from Z $\to \ell^{\pm}\ell^{\mp}$ (dashed-dotted line). The lower plot shows the same distribution for events passing the cut $\mathrm{E}_{\ell\ell} > 100$ GeV.

dilepton pair: requiring $\mathrm{E}_{\ell\ell} > 100$ GeV, the contributions from the other decays are almost totally suppressed, and the total distribution corresponds almost completely to the distribution of signal events.

Table 4 shows, for each SM process, the cross section given by `PYTHIA 6.152`, the number of produced events, and the number of events for each stage of the selection procedure. The number of produced $\mathrm{t\bar{t}}$ events corresponds to the number of events expected in 10 fb^{-1} of integrated luminosity at LHC; for the other processes, the cross section is too large to allow the production of an equivalent sample and smaller samples have been produced. W+jets and QCD samples are completely suppressed by the requirement of isolation on the leptons. Even if these are limited samples, it is reasonable to expect that these channels will not significantly affect the final study also in a real data analysis. The surviving Z+jets and $\mathrm{t\bar{t}}$ events have instead to be included in the dilepton invariant mass plot with the correct normalization factor.

In Fig. 4 the same flavour opposite sign dilepton pair invariant mass distribution is shown for SUSY events superimposed over the SM background. The $\mathrm{t\bar{t}}$ sample gives a wide distribution, while the Z+jets channel is distinguishable for the Z peak which lies quite close to the end-point of the SUSY distribution. In order to further reduce the SM background, the higher $E_{\mathrm{T}}^{\mathrm{miss}}$ content of SUSY events can be exploited. Indeed, as can be seen in Fig. 5, which shows the dilepton invariant mass distributions for different $E_{\mathrm{T}}^{\mathrm{miss}}$ cuts, SM background can be efficiently rejected imposing a cut $E_{\mathrm{T}}^{\mathrm{miss}} > 150$ GeV.

The SM background and the tail in SUSY event distribution can be further eliminated by subtracting the invariant mass of different flavour opposite sign lepton pairs.

Finally, a fit with a jacobian function can be performed on the clean $\mathrm{M(e^+e^-)+M(\mu^+\mu^-)-M(e^+\mu^-)-M(\mu^+e^-)}$ distribution to evaluate $\mathrm{M}_{\ell\ell}^{\mathrm{max}}$. The result is shown in Fig. 6. The value obtained is

$$\mathrm{M}_{\ell^+\ell^-}^{\mathrm{max}} = \frac{\sqrt{\left(\mathrm{M}^2_{\tilde{\chi}_2^0} - \mathrm{M}^2_{\tilde{\ell}}\right)\left(\mathrm{M}^2_{\tilde{\ell}} - \mathrm{M}^2_{\tilde{\chi}_1^0}\right)}}{\mathrm{M}_{\tilde{\ell}}} = (78.9 \pm 2.1)\ \mathrm{GeV/c^2} \tag{6}$$

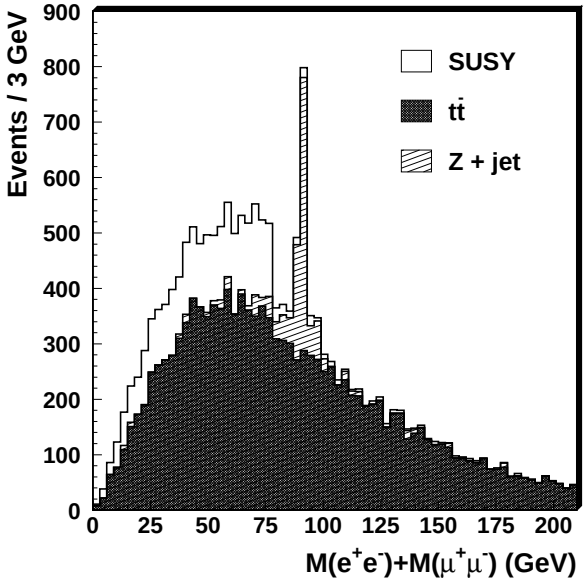

Figure 4: Invariant mass distribution of same flavour opposite sign isolated leptons for SUSY events, superimposed on the SM background. Contributions from $\mathrm{t\bar{t}}$ and Z+jets events are shown separately.

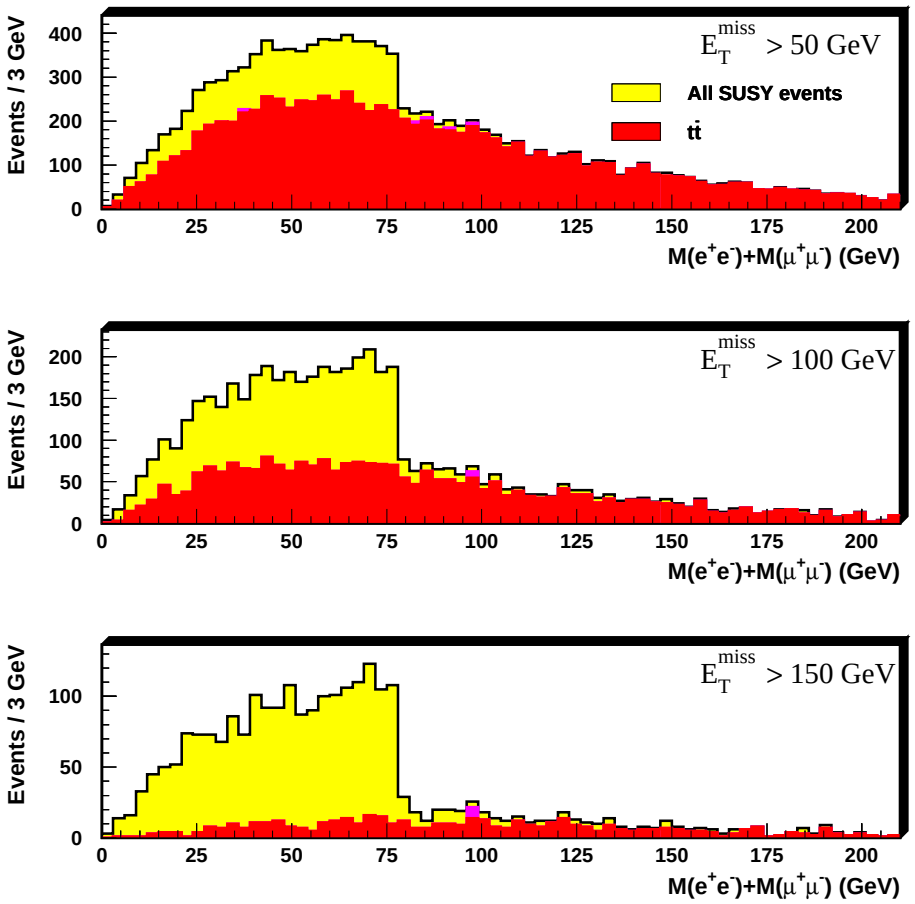

Figure 5: Same flavour opposite sign lepton pair invariant mass distribution for $E_{\mathrm{T}}^{\mathrm{miss}} > 50$ GeV (up), $E_{\mathrm{T}}^{\mathrm{miss}} > 100$ GeV (centre) and $E_{\mathrm{T}}^{\mathrm{miss}} > 150$ GeV (down).

Table 4: Considered SM processes. For each background source, the cross section as given by PYTHIA 6.152 is shown. The number of produced events and the number of events surviving the sequence of selection criteria for sbottom reconstruction, as described in the text, are also shown.

	σ (pb)	N produced events	2 leptons	2 b jets	2 SFOS isol. ℓ
$t\bar{t}$	6.21×10^2	6.21×10^6	886809	140552	14525
$Z + jets$ ($\hat{p}_T > 60$ GeV/c)	2.87×10^3	3.89×10^6	172894	1322	161
$W + jets$ ($\hat{p}_T > 60$ GeV/c)	7.51×10^3	2.60×10^6	5850	37	0
QCD ($\hat{p}_T$ bin)					
$50 \div 100$ GeV/c	2.86×10^7	1.90×10^6	460	30	0
$100 \div 200$ GeV/c	1.64×10^6	1.90×10^6	3366	304	0
$200 \div 300$ GeV/c	6.67×10^4	1.90×10^6	11395	1217	0
$300 \div 400$ GeV/c	8.57×10^3	1.90×10^6	19892	2201	0
$400 \div 500$ GeV/c	1.82×10^3	1.90×10^6	28149	2945	0
> 500 GeV/c	8.19×10^2	1.90×10^6	39902	4101	0

which is in very good agreement with the true value of 78.16 GeV/c^2.

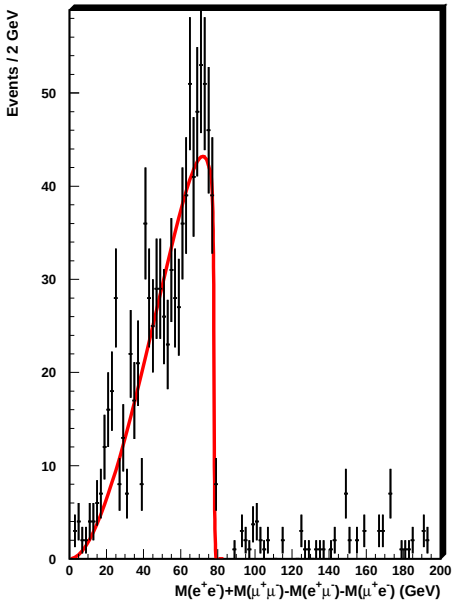

Figure 6: Distribution of $M(e^+e^-) + M(\mu^+\mu^-) - M(e^+\mu^-) - M(\mu^+e^-)$ for SUSY and SM events passing the cuts $E_T^{miss} > 150$ GeV and $E_{\ell\ell} > 100$ GeV. The result of a jacobian fit is shown.

To reconstruct the sbottom, opposite charge leptons in a window of about 15 GeV/c^2 around the edge are selected. This requirement allows to select a kinematical condition in which the leptons are emitted back-to-back in the $\tilde{\chi}_2^0$ rest frame, with the $\tilde{\chi}_1^0$ at rest. In this condition the $\tilde{\chi}_2^0$ momentum is reconstructed through the relation:

$$\tilde{p}_{\tilde{\chi}_2^0} = \left(1 + \frac{m_{\tilde{\chi}_1^0}}{M_{\ell^+\ell^-}}\right) \tilde{p}_{\ell^+\ell^-}. \quad (7)$$

The mass of the $\tilde{\chi}_1^0$ is taken from the Monte Carlo. The dependece of the sparticle masses from the $\tilde{\chi}_1^0$ mass is discussed in Sec. 5. The $\tilde{\chi}_2^0$ from the dilepton distribution has to be associated to one of the b jets in the event to have the sbottom from the $\tilde{b} \to \tilde{\chi}_2^0 b$: the most energetic b jet has been chosen since, according to the parton level distributions, the b quarks produced in the $\tilde{b} \to \tilde{\chi}_2^0 b$ decay have a harder spectrum than the others. The $\tilde{\chi}_2^0 b$ invariant mass shows a clear bump at about 500 GeV/c^2, the region in which we expect to find the sbottom, emerging over a wide SUSY background distribution, mainly due to combinatorics, as illustrated in Fig. 7 (solid

line).

The main combinatorial sources can be grouped into two families:

- events in which the right decay chain is present, but where the $\tilde{\chi}_2^0$ reconstructed from the dilepton pair is associated to a b not coming from the sbottom. This source can be reduced if the b associated to the $\tilde{\chi}_2^0$ arises from a gluino, from a stop or from a top, since these b quarks show a softer spectrum than b quarks produced in sbottom decays;
- events in which the right decay chain is not present, but a $\tilde{\chi}_2^0$ produced by other sparticles can be associated to other b jets. This source can be hardly reduced since no difference can be observed between $\tilde{\chi}_2^0$'s coming from sbottom and other $\tilde{\chi}_2^0$'s.

As shown in Fig. 7, a lower cut on the energy of the most energetic b jet can therefore reduce the first source of combinatorics.

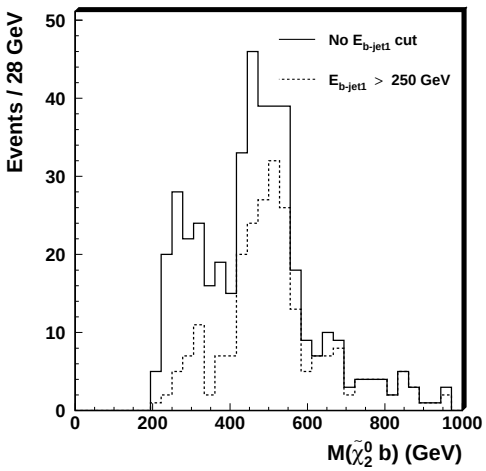

Figure 7: Sbottom mass peak for events having $65\ \mathrm{GeV/c^2} < \mathrm{M}_{\ell\ell} < 80\ \mathrm{GeV/c^2}$. No cut on the energy of the most energetic jet (solid line), and $\mathrm{E}_{b1} > 250\ \mathrm{GeV}$ effects are compared.

In order to extract the sbottom mass (Fig. 8), a Gaussian fit is performed on the peak together with a polynomial to take into account the combinatorial and Standard Model background. The result is

$$\mathrm{M}(\tilde{\chi}_2^0\mathrm{b}) = (500 \pm 7)\ \mathrm{GeV/c^2} \quad (8a)$$

$$\sigma = (42 \pm 5)\ \mathrm{GeV/c^2} \quad (8b)$$

where the error is only statistical, given by the fit, and σ is the width of the Gaussian. The physical widths of the sbottoms are $\Gamma_{\tilde{\mathrm{b}}_1} = 2.8$ GeV/c^2, $\Gamma_{\tilde{\mathrm{b}}_2} = 1.4$ GeV/c^2. The measured width is much larger, and determined essentially by instrumental effects. The masses of the generated particles are $\mathrm{M}(\tilde{\mathrm{b}}_1) = 496.0$ GeV/c^2, $\mathrm{M}(\tilde{\mathrm{b}}_2) = 524.0$ GeV/c^2. The fit is performed on the unresolved peak, but the result is in good agreement with both the sbottom masses. It can be further considered that a larger number of events with $\tilde{\mathrm{b}}_1$ than with $\tilde{\mathrm{b}}_2$ is expected. In fact, the $\sigma \times \mathrm{BR}$ for sbottoms directly produced or arising from gluino decays and hence going into the searched chain is larger for $\tilde{\mathrm{b}}_1$. More precisely:

$$\sigma \times \mathrm{BR}(\mathrm{pp} \to \tilde{\mathrm{g}} \to \tilde{\mathrm{b}}_1 \to \tilde{\chi}_2^0 \to \tilde{\ell}_\mathrm{R}^\pm \ell^\mp \to \tilde{\chi}_1^0 \ell^\pm \ell^\mp) = 449.9\ \mathrm{fb} \quad (9a)$$

$$\sigma \times \mathrm{BR}(\mathrm{pp} \to \tilde{\mathrm{b}}_1 \to \tilde{\chi}_2^0 \to \tilde{\ell}_\mathrm{R}^\pm \ell^\mp \to \tilde{\chi}_1^0 \ell^\pm \ell^\mp) = 85.5\ \mathrm{fb} \quad (9b)$$

$$\sigma \times \mathrm{BR}(\mathrm{pp} \to \tilde{\mathrm{g}} \to \tilde{\mathrm{b}}_2 \to \tilde{\chi}_2^0 \to \tilde{\ell}_\mathrm{R}^\pm \ell^\mp \to \tilde{\chi}_1^0 \ell^\pm \ell^\mp) = 179.7\ \mathrm{fb} \quad (9c)$$

$$\sigma \times \mathrm{BR}(\mathrm{pp} \to \tilde{\mathrm{b}}_2 \to \tilde{\chi}_2^0 \to \tilde{\ell}_\mathrm{R}^\pm \ell^\mp \to \tilde{\chi}_1^0 \ell^\pm \ell^\mp) = 31.5\ \mathrm{fb} \quad (9d)$$

so the total $\sigma \times$ BR's are 535.1 fb for $\tilde{\mathrm{b}}_1$ and 211.1 fb for $\tilde{\mathrm{b}}_2$. These two quantities are shortly indicated as $\sigma \times \mathrm{B}R(\tilde{\mathrm{b}}_1)$ and $\sigma \times \mathrm{B}R(\tilde{\mathrm{b}}_2)$. Under the assumption that the unresolved peak is due to the superposition of the

$\tilde{b}_1$ and $\tilde{b}_2$ peaks, each weighted by the corresponding $\sigma \times BR$, the expected mass should be:

$$\bar{M}(\tilde{b}) = \frac{M(\tilde{b}_1) \cdot \sigma \times BR(\tilde{b}_1) + M(\tilde{b}_2) \cdot \sigma \times BR(\tilde{b}_2)}{\sigma \times BR(\tilde{b}_1) + \sigma \times BR(\tilde{b}_2)} = 503.9 \text{ GeV/c}^2 \quad (10)$$

which is in good agreement with the result of the fit within the error. Of course this is only a rough estimate, but it can be useful to evaluate the effectiveness of the reconstruction method by comparing the result with the expected value. It can be concluded that CMS will be able to start to identify a sbottom within its first year of life, if the Supersymmetric scenario will be favourable like point B.

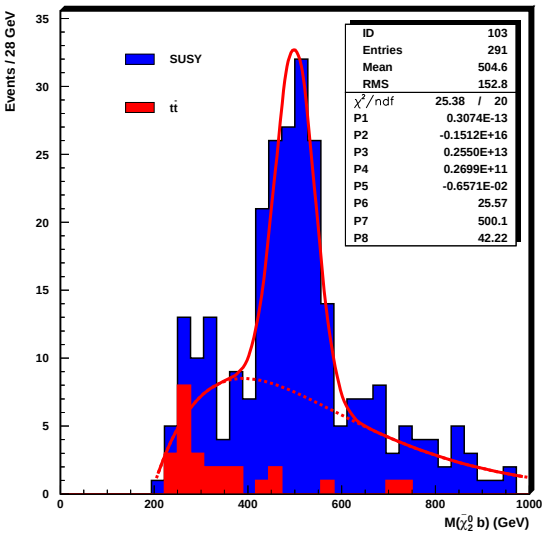

Figure 8: Result of the fit for the reconstructed sbottom: a Gaussian is used for the signal peak, whereas the combinatorial and Standard Model background are fitted with a polynomial. The measured mass of the sbottom is $M(\tilde{\chi}_2^0 b) = (500 \pm 7)$ GeV/c^2, the resolution of the peak is $\sigma = 42 \pm 5$ GeV/c^2, corresponding to 8.4% of the mass. Events are selected requiring $65 \text{ GeV/c}^2 < M_{\ell\ell} < 80 \text{ GeV/c}^2$, $E_T^{miss} > 150$ GeV, $E_{b1} > 250$ GeV.

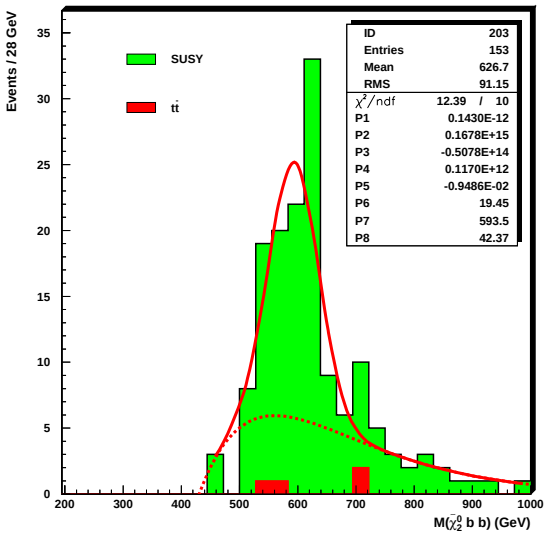

Figure 9: Result of the fit for the reconstructed gluino: a Gaussian is used for the signal peak, whereas the combinatorial and Standard Model background are fitted with a polynomial. The measured mass of the gluino is $M(\tilde{\chi}_2^0 b) = (594 \pm 7)$ GeV/c^2, the resolution of the peak is $\sigma = 42 \pm 7$ GeV/c^2, corresponding to 5.5% of the mass. Events are selected requiring $65 \text{ GeV/c}^2 < M_{\ell\ell} < 80 \text{ GeV/c}^2$, $E_T^{miss} > 150$ GeV, $E_{b1} > 250$ GeV, $400 \text{ GeV/c}^2 < M(\tilde{\chi}_2^0 b) < 600 \text{ GeV/c}^2$.

3 Reconstruction of $\tilde{g} \to \tilde{b}b$ at Point B

In order to reconstruct the gluino, the reconstructed sbottom should be associated to another b jet. More than 86% of events have only two jets. For events having more than two b jets we choose the b jet closest in angle to the reconstructed sbottom. Figure 9 refers to the gluino peak as attained imposing $E_T^{miss} > 150$ GeV and $E_{b1} > 250$ GeV. In addition, only the events in the sbottom peaks are selected, requiring $400 \text{ GeV/c}^2 < M(\tilde{\chi}_2^0 b) < 600 \text{ GeV/c}^2$, corresponding approximately to the central value $\pm 2.5\sigma$.

A Gaussian fit superimposed on a polynomial to take into account the combinatorial plus Standard Model background is performed on the distribution. The corresponding result is

$$M(\tilde{\chi}_2^0 bb) = (594 \pm 7) \text{ GeV/c}^2 \quad (11a)$$

$$\sigma = (42 \pm 7) \text{ GeV/c}^2 \quad (11b)$$

in good agreement with the generated mass value for the gluino, $M(\tilde{g}) = 595$ GeV/c^2. Again, the physical width of the particle, $\Gamma_{\tilde{g}} = 7.78$ GeV/c^2, is much smaller than the width of the observed peak, which is due uniquely to resolution effects.

4 Squark reconstruction at Point B

In this section the reconstruction procedure used for the supersymmetric partners of the light quarks ($\tilde{u}$, $\tilde{d}$, $\tilde{c}$ and $\tilde{s}$) is described. They can be reconstructed with a method similar to the one used for the sbottoms, looking at the decay chain:

$$\begin{aligned} \tilde{q} \quad \rightarrow \quad & \tilde{\chi}_2^0 q \\ & \downarrow \\ & \tilde{\ell}_R^{\pm} \ell^{\mp} \rightarrow \tilde{\chi}_1^0 \ell^{\pm} \ell^{\mp} \end{aligned} \tag{12}$$

which is identical to the chain considered in the case of the sbottom, apart from the emission of a light quark q instead of a bottom in the decay $\tilde{q} \rightarrow \tilde{\chi}_2^0 q$. Non b jets have to be identified, and the b-tagging capability of the CMS detector has hence to be used in order to veto the presence of b jets and to perform an anti b tagging.

Squark direct production has a large cross section, comparable to the gluino production one. The reconstruction method developed to observe the sbottom has hence to be adjusted to take care of the fact that $\tilde{q}\tilde{q}$ and $\tilde{q}\tilde{g}$ production processes cannot be neglected. The $\sigma \times$ BR's for the squarks directly produced in proton-proton collisions and hence decaying into the whole chain are

$$\sigma \times \mathrm{BR}(pp \rightarrow \tilde{q}_R \rightarrow \mathrm{decaychain}) = 31\ \mathrm{fb} \tag{13a}$$

$$\sigma \times \mathrm{BR}(pp \rightarrow \tilde{q}_L \rightarrow \mathrm{decaychain}) = 1.413\ \mathrm{pb}. \tag{13b}$$

The $\sigma \times$ BR for the right squarks is two orders of magnitude smaller than the one of the left squarks due to the smaller branching ratio of the decay $\tilde{q}_R \rightarrow \tilde{\chi}_2^0 q$, which is only 1%, versus the 30% branching ratio of the $\tilde{q}_L \rightarrow \tilde{\chi}_2^0 q$. As a consequence of this, the right squarks are hardly visible, and the following reconstruction method refers to the left squarks. This can be considered an advantage: unlike the sbottom case, the reconstructed peak is not the superposition of two peaks, and it is therefore possible to measure more accurately the mass of the left squark. On the other side, it is practically impossible to observe right squarks, since 99% of their decays produce a quark and an undetectable $\tilde{\chi}_1^0$. So, if supersymmetry will reveal itself with a pattern similar to point B, it will be very hard to get information about the right component of squarks which are not sbottoms or stops.

As in the case of the sbottom reconstruction, not only the squark directly produced in the collisions have to be considered, but also the ones coming from gluino decay:

$$\begin{aligned} \tilde{g} \quad \rightarrow \quad & \tilde{q} q \\ & \downarrow \\ & \tilde{\chi}_2^0 q \\ & \downarrow \\ & \tilde{\ell}_R^{\pm} \ell^{\mp} \rightarrow \tilde{\chi}_1^0 \ell^{\pm} \ell^{\mp}. \end{aligned} \tag{14}$$

The $\sigma \times$ BR of squarks produced in gluino decays can be easily calculated:

$$\sigma \times \mathrm{BR}(pp \rightarrow \tilde{g} \rightarrow \tilde{q}_R \rightarrow \mathrm{decaychain}) = 39\ \mathrm{fb} \tag{15a}$$

$$\sigma \times \mathrm{BR}(pp \rightarrow \tilde{g} \rightarrow \tilde{q}_L \rightarrow \mathrm{decaychain}) = 0.533\ \mathrm{pb}. \tag{15b}$$

Again, the probability that right squarks can give the wanted chain is much smaller than for left squarks. Given the very high $\sigma \times$BR for squarks going into the $\tilde{\chi}_2^0$-dilepton chain, which is about four times larger than for the sbottom chain, it is plausible to try the reconstruction with an integrated luminosity lower than the 10 fb^{-1} considered in the previous paragraphs. The following plots refer to an integrated luminosity of 1 fb^{-1}, corresponding to the first two or three months of life of the Large Hadron Collider, according to present expectations.

The events are selected requiring:

- at least two same flavour opposite sign (SFOS) isolated leptons, with $p_T > 15$ GeV/c and $|\eta| < 2.4$; as in the previous sections, for leptons we mean only electrons and muons;
- at least two jets, tagged as non b jets, with $p_T > 20$ GeV/c and $|\eta| < 2.4$;
- no b jets.

The jets are considered not coming from b if the b-tagging parameter defined in Ref. [9] is less than 2. The third condition of the list is a *b veto*: all the events having at least one jet recognized as a b jet are rejected. This is useful to suppress most of the events with sbottoms or stops, which could be one of the main source of SUSY background for the reconstruction of the squarks.

In Table 5 the number of events surviving the various steps of the selection is shown, for an initial sample corresponding to 1 fb^{-1}.

Table 5: Number of produced SUSY events. For each generation process, the number of events surviving the sequence of selection criteria for squark reconstruction, as described in the text, is shown.

	N ev in 1 fb^{-1}	2 leptons	b veto	2 non b jets	2 SFOS isol. ℓ
$\tilde{\mathrm{b}}\tilde{\mathrm{b}}$	515	204	55	41	8
$\tilde{\mathrm{b}}\tilde{\mathrm{g}}$	706	245	68	57	25
$\tilde{\chi}\tilde{\chi}$	1899	253	238	15	7
$\tilde{\chi}\tilde{\mathrm{g}}$	476	92	42	16	12
$\tilde{\chi}\tilde{\mathrm{q}}$	1888	272	247	112	59
$\tilde{\mathrm{g}}\tilde{\mathrm{g}}$	6994	1473	438	395	129
$\tilde{\ell}\tilde{\ell}$	537	110	110	3	3
$\tilde{\mathrm{q}}\tilde{\mathrm{b}}$	361	90	39	27	16
$\tilde{\mathrm{q}}\tilde{\mathrm{g}}$	28319	4078	2024	1742	743
$\tilde{\mathrm{q}}\tilde{\mathrm{q}}$	14160	1209	1050	820	444
$\tilde{\mathrm{t}}\tilde{\mathrm{t}}$	1831	489	120	80	15
Total	57686	8515	4431	3318	1461

The main contributions are from $\tilde{\mathrm{q}}\tilde{\mathrm{q}}$, $\tilde{\mathrm{q}}\tilde{\mathrm{g}}$ and $\tilde{\mathrm{g}}\tilde{\mathrm{g}}$ events. A sketch of the decay chains given by such processes is shown in Fig. 10. This is a pictorial representations of the decays, where only some possibilities have been considered: it is possible that the $\tilde{\chi}_2^0$ giving the lepton pair, in $\tilde{\mathrm{q}}\tilde{\mathrm{g}}$ comes from the squark rather than the gluino, or that in $\tilde{\mathrm{g}}\tilde{\mathrm{g}}$ not both gluinos decay into a squark, but one of them produce a sbottom or a stop. There are tens of possible combinations, which are not graphically represented. The treatment of the combinatorial is crearly more difficult than for the sbottom chain.

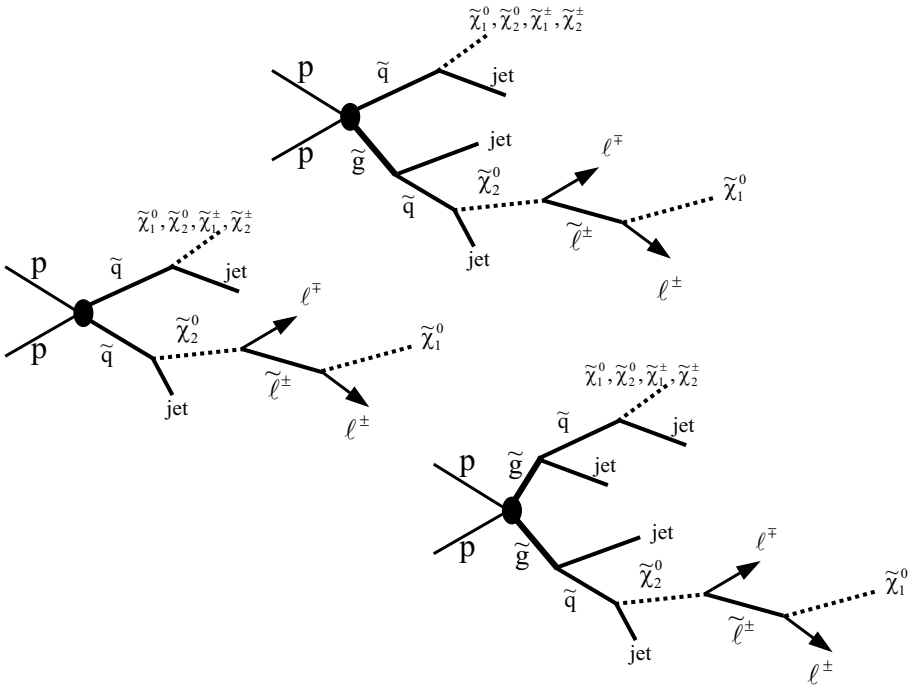

Figure 10: A pictorial view of the decay chains of interest for the squark reconstruction, in $\tilde{\mathrm{q}}\tilde{\mathrm{q}}$, $\tilde{\mathrm{q}}\tilde{\mathrm{g}}$ and $\tilde{\mathrm{g}}\tilde{\mathrm{g}}$ events.

Table 6 shows the number of Standard Model events surviving the same selection criteria. The main contributions are from $t\bar{t}$ and Z+jets. All the other possible background sources are negligible: the most effective cut is the requirement of isolation on the leptons.

Table 6: Considered SM processes. For each background source, the cross section as given by PYTHIA 6.152 is shown. The number of produced events and the number of events surviving the sequence of selection criteria for squark reconstruction, as described in the text, are also shown.

	σ (pb)	N produced events	2 leptons	b veto	2 non b jets	2 SFOS isol. ℓ
$t\bar{t}$	6.21×10^2	6.21×10^5	88561	33410	16853	1415
$Z + jets$ ($\hat{p}_T > 60$ GeV/c)	2.87×10^3	3.89×10^6	172894	159479	17205	13138
$W + jets$ ($\hat{p}_T > 60$ GeV/c)	7.51×10^3	2.60×10^6	4517	3869	738	2
QCD ($\hat{p}_T$ bin)						
$50 \div 100$ GeV/c	2.86×10^7	1.90×10^6	460	270	78	0
$100 \div 200$ GeV/c	1.64×10^6	1.90×10^6	3366	1658	965	0
$200 \div 300$ GeV/c	6.67×10^4	1.90×10^6	11395	5394	4088	0
$300 \div 400$ GeV/c	8.57×10^3	1.90×10^6	19892	9545	7954	1
$400 \div 500$ GeV/c	1.82×10^3	1.90×10^6	28149	13961	11832	2
> 500 GeV/c	8.19×10^2	1.90×10^6	39902	20343	17581	0

The same conceptual steps of the sbottom reconstruction are followed: the same flavour opposite sign lepton pair invariant mass is first built, in order to observe the end-point and hence to get the $\tilde{\chi}_2^0$ momentum. Selecting events in the window 65 GeV/c^2 $< M_{\ell\ell} <$ 80 GeV/c^2, the same region used for the sbottom reconstruction, and associating the most energetic jet to the $\tilde{\chi}_2^0$, whose momentum is evaluated using the Eq. (7), an invariant mass distribution is built where a clean peak can be observed in the region where the squark is expected. In Fig. 11 this peak is shown superimposed over the Standard Model background for three different values of E_T^{miss} cut. Requiring $E_T^{miss} > 100$ GeV is enough to keep SM events at an acceptable level.

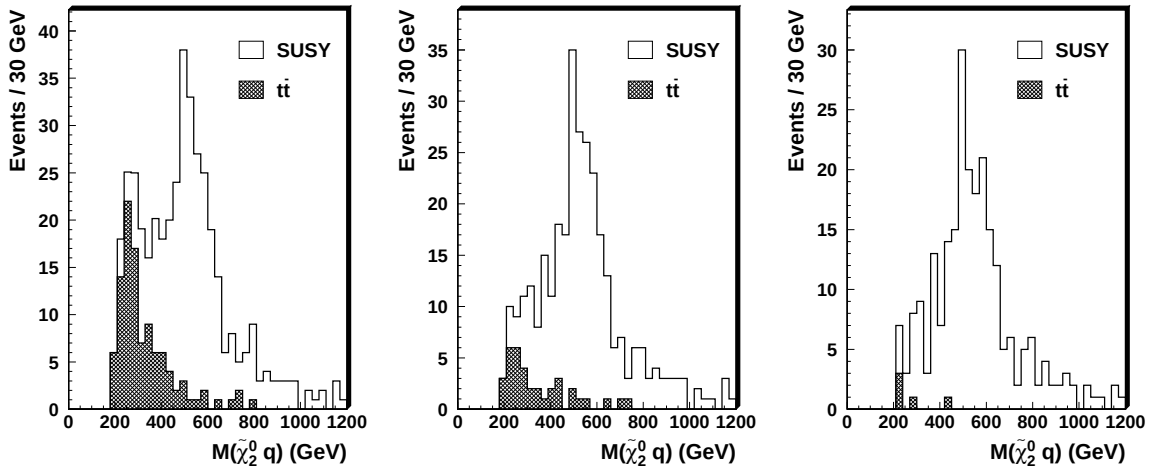

Figure 11: Squark mass peak for SUSY over the Standard Model background for $E_T^{miss} > 50$ GeV (left), $E_T^{miss} > 100$ GeV (centre), $E_T^{miss} > 150$ GeV (right), for events with $65\ \mathrm{GeV/c^2} < M_{\ell\ell} < 80\ \mathrm{GeV/c^2}$. The integrated luminosity is 1 fb^{-1}.

In Fig. 12 a Gaussian plus a polynomial fit is performed on the squark peak. The result of the fit is

$$M(\tilde{\chi}_2^0 q) = 536 \pm 10\ \mathrm{GeV/c^2} \quad (16a)$$

$$\sigma[M(\tilde{\chi}_2^0 q)] = 60 \pm 9\ \mathrm{GeV/c^2} \quad (16b)$$

where the errors are only statistical. The measured mass should be compared to the mean weighted on the $\sigma \times BR$

of the $\tilde{q}_L$ and $\tilde{q}_R$, as already done for the sbottom. Since the $\sigma \times BR$ of the $\tilde{q}_R$ is only 3% of the total, it nevertheless results:

$$\bar{M}(\tilde{q}) \approx M(\tilde{q}_L) \tag{17}$$

thus the measured mass can be compared to the true masses of the left squarks:

$$M(\tilde{d}_L) = M(\tilde{s}_L) = 542.8\ \mathrm{GeV}/c^2 \tag{18a}$$

$$M(\tilde{u}_L) = M(\tilde{c}_L) = 537.0\ \mathrm{GeV}/c^2 \tag{18b}$$

resulting in agreement within the error. Of course it is not possible to observe up-type and down-type squarks separately, for their mass being so close, as well as it is not possible to estimate experimentally the physical width of the squarks: the width of the peak is due only to resolution effects, and is much larger than $\Gamma_{\tilde{q}_L} = 5\ \mathrm{GeV}/c^2$. Nonetheless the collected statistics is sufficient to measure the mass of the squark even at 1 fb^{-1}. This means that in favourable conditions, CMS will be able to perform a preliminary spectroscopy on supersymmetric particles in an early phase of operation.

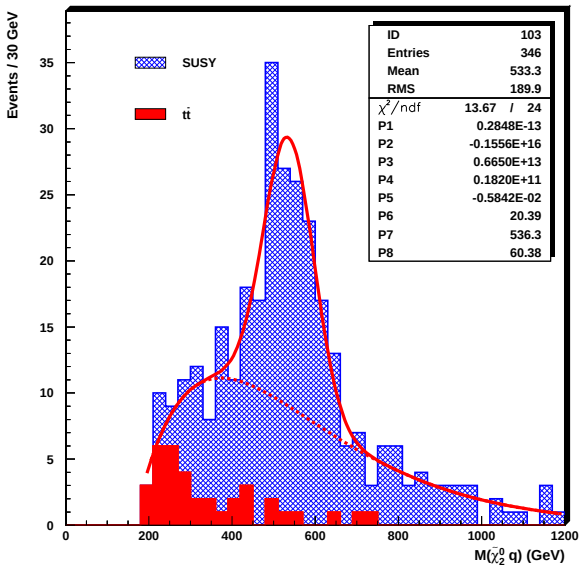

Figure 12: Distribution of invariant mass of $\tilde{\chi}_2^0$ and the most energetic jet for events with 65 $\mathrm{GeV}/c^2 < M_{\ell\ell} < 80\ \mathrm{GeV}/c^2$, and $E_T^{miss} > 100$ GeV. The integrated luminosity is 1 fb^{-1}. The peak is fitted with a Gaussian plus a polynomial which takes into account the Standard Model and combinatorial background.

The treatment of the combinatorial background is more complicated than for the sbottom: the main production processes are $\tilde{q}\tilde{g}$, $\tilde{g}\tilde{g}$ and $\tilde{q}\tilde{q}$. Most of the events have therefore two squarks and a higher jet multiplicity. However, similarly to the sbottom case, a lower cut on the energy of the most energetic jet allows a good combinatorial reduction. Figure 13 shows the squark peak for $E_{j1} > 300$ GeV, for a sample corresponding to 10 fb^{-1} of integrated luminosity. The measured values are

$$M(\tilde{\chi}_2^0 q) = 535 \pm 3\ \mathrm{GeV}/c^2 \tag{19a}$$

$$\sigma[M(\tilde{\chi}_2^0 q)] = 57 \pm 3\ \mathrm{GeV}/c^2. \tag{19b}$$

The jet energy cut has not been applied also to the 1 fb^{-1} because of the insufficient statistics. The resolution of the $\sigma \times BR$ of the entire squark production and decay process can be inferred by the number of events in the peak, which is 630, leading to a value:

$$\frac{\delta(\sigma \times BR)}{\sigma \times BR} = 4\%. \tag{20}$$

If the $M(\tilde{\chi}_1^0) = M_{\ell\ell}^{max}$ assumption is used, the fit results are

$$M(\tilde{\chi}_2^0 q) = 502 \pm 3\ \mathrm{GeV}/c^2 \tag{21a}$$

$$\sigma[M(\tilde{\chi}_2^0 q)] = 56 \pm 3\ \mathrm{GeV}/c^2. \tag{21b}$$

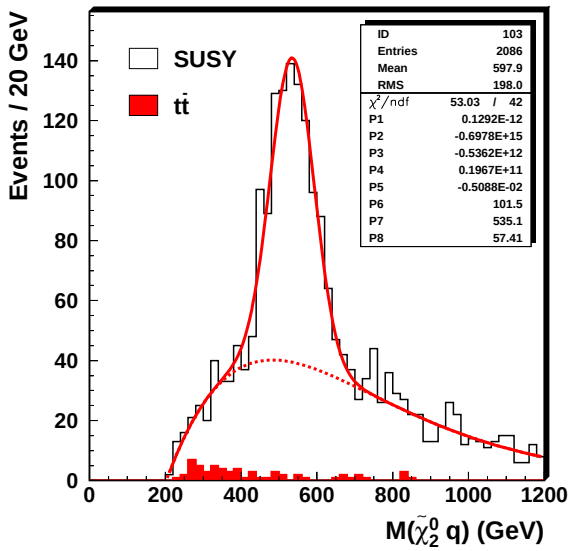

Figure 13: Invariant mass of the system $\tilde{\chi}_2^0$q for an integrated luminosity of 10 fb^{-1}. Events are selected having 65 GeV/c^2 $<$ M$_{\ell\ell}$ $<$ 80 GeV/c^2, $E_{\mathrm{T}}^{\mathrm{miss}} >$ 100 GeV and E$_{\mathrm{j1}} >$ 300 GeV. A fit is performed with a Gaussian superimposed over a polynomial to take into account the combinatorial plus Standard Model background.

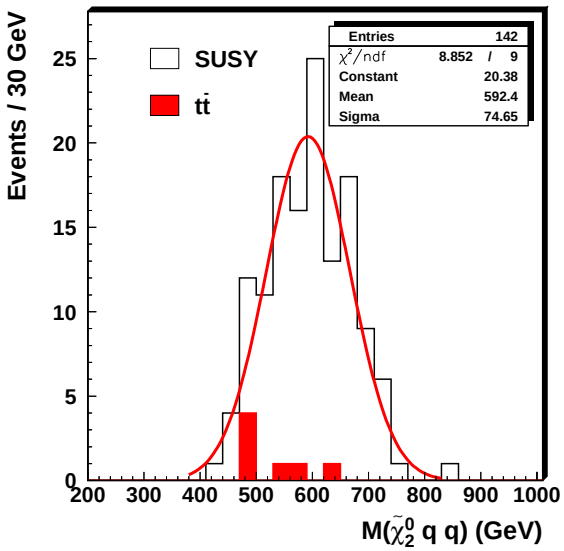

Figure 14: Invariant mass of the system $\tilde{\chi}_2^0$qq for events having 65 GeV/c^2 $<$ M$_{\ell\ell}$ $<$ 80 GeV/c^2, $E_{\mathrm{T}}^{\mathrm{miss}} >$ 50 GeV, E$_{\mathrm{j1}} >$ 300 GeV, 390 GeV/c^2 $<$ M$(\tilde{\chi}_2^0\mathrm{q}) <$ 690 GeV/c^2 and E$_{\mathrm{j2}} <$ 60 GeV. The integrated luminosity is 10 fb^{-1}.

The gluino peak can be observed also in the squark decay chain with a procedure similar to the one used for the sbottom: after removing the most energetic jet form the list of available jets, the one closest in angle to the reconstructed squark is associated to it. The $\tilde{\chi}_2^0$jj invariant mass presents a wide tail on the right due mainly to wrong association with high energetic jets arising from squarks. An upper cut on the energy of the second jet can strongly reduce this source of combinatorial and allow an acceptable gluino peak shape. A detailed description of the combinatorial treatment can be found in Ref. [6]. Figure 14 shows the final gluino peak, after a cut E$_{\mathrm{j2}} <$ 60 GeV is applied on the second jet. The Gaussian fit gives:

$$\mathrm{M}(\tilde{\chi}_2^0\mathrm{qq}) = 592 \pm 7\ \mathrm{GeV/c^2} \quad (22a)$$

$$\sigma[\mathrm{M}(\tilde{\chi}_2^0\mathrm{qq})] = 75 \pm 5\ \mathrm{GeV/c^2} \quad (22b)$$

which is in agreement with the mass value of the generated gluino: M$(\tilde{\mathrm{g}}) = 595.1$ GeV/c^2. Although the achieved resolution is worse than the one of the gluino reconstructed into the sbottom chain, this results is remarkable since it has been obtained in a totally independent way. In the same figure, the peak is compared to the peak obtained assuming M$(\tilde{\chi}_1^0) = \mathrm{M}_{\ell\ell}^{\mathrm{max}}$. The result of the fit is

$$\mathrm{M}(\tilde{\chi}_2^0\mathrm{qq}) = 567 \pm 8\ \mathrm{GeV/c^2} \quad (23a)$$

$$\sigma[\mathrm{M}(\tilde{\chi}_2^0\mathrm{qq})] = 77 \pm 6\ \mathrm{GeV/c^2} \quad (23b)$$

the measurement of the mass is hence left-shifted by 25 GeV/c^2.

5 Dependence from the M$(\tilde{\chi}_1^0)$

All the results shown in the previous sections are obtained in the hypothesis of a known $\tilde{\chi}_1^0$ mass. In a realistic scenario, however, CMS will not be able to detect $\tilde{\chi}_1^0$, this being a weakly interacting particle which escapes the detector. In order to evaluate the impact of the uncertainty in M$(\tilde{\chi}_1^0)$ on the mass resolution of sbottom and gluino, the analysis has been repeated taking as an approximate value for M$(\tilde{\chi}_1^0)$ the dilepton end-point value. In a mSUGRA scenario, in fact, M$(\tilde{\chi}_2^0) \sim 2\mathrm{M}(\tilde{\chi}_1^0)$ and hence $\mathrm{M}_{\ell^+\ell^-}^{\mathrm{max}} \sim \mathrm{M}(\tilde{\chi}_2^0) - \mathrm{M}(\tilde{\chi}_1^0) \sim \mathrm{M}(\tilde{\chi}_1^0)$.

In Fig. 15 the shift in the sbottom and gluino mass peak due to this effect is shown.
The measured mass values for sbottom and gluino are

$$\mathrm{M}(\tilde{\chi}_2^0\mathrm{b})_{\mathrm{M}(\tilde{\chi}_1^0)\approx \mathrm{M}^{\max}_{\ell^+\ell^-}} = 470 \pm 6\ \mathrm{GeV/c^2} \quad (24a)$$

$$\mathrm{M}(\tilde{\chi}_2^0\mathrm{bb})_{\mathrm{M}(\tilde{\chi}_1^0)\approx \mathrm{M}^{\max}_{\ell^+\ell^-}} = 555 \pm 6\ \mathrm{GeV/c^2}. \quad (24b)$$

The peaks are shifted by about 30 GeV/c^2 in the case of the sbottom and by about 40 GeV/c^2 for the gluino. The error on the measured mass introduced by this approximation is therefore:

$$\frac{\delta(\mathrm{M}(\tilde{\chi}_2^0\mathrm{b}))}{\mathrm{M}(\tilde{\chi}_2^0\mathrm{b})} = 6.0\% \qquad \frac{\delta(\mathrm{M}(\tilde{\chi}_2^0\mathrm{bb}))}{\mathrm{M}(\tilde{\chi}_2^0\mathrm{bb})} = 6.7\%. \quad (25)$$

The error due to the indetermination of $\mathrm{M}(\tilde{\chi}_1^0)$ is hence much larger than the statistical error at 10 fb^{-1}.

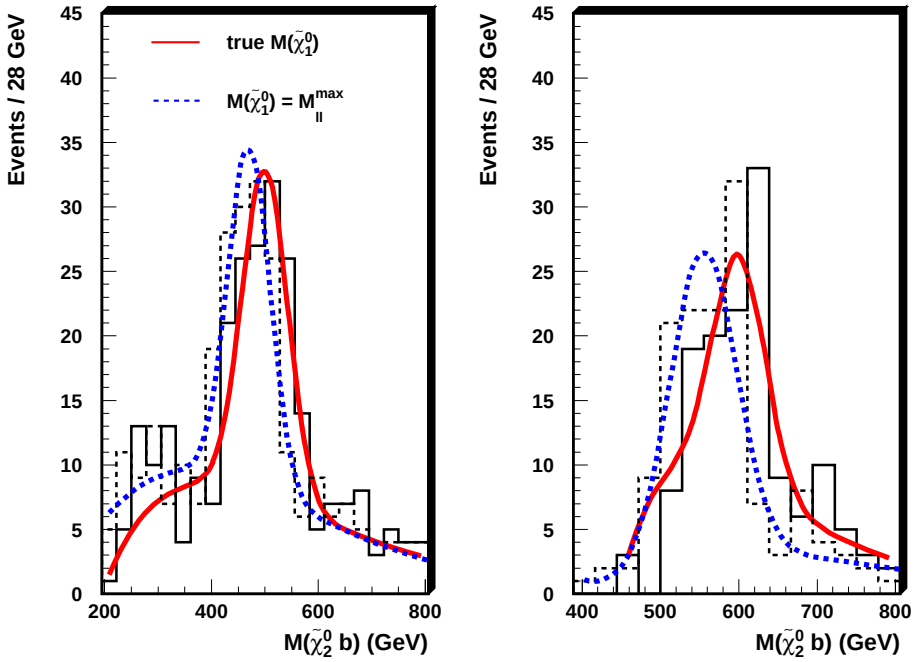

Figure 15: Comparison between the fit done on the sbottom (left) and gluino (right) peaks built assuming the true $\tilde{\chi}_1^0$ mass value (red-light grey curve - solid histogram) or approximating it with the maximum of the dilepton distribution taken from the fit (blue-dark grey curve - dashed histogram).

Indeed, it should be noticed, that in real life mSUGRA could not be the correct model, and so in order to get model independent information other strategies should be used. One possibility is the one already exploited in ref. [10, 11], which make use of several different end-points, in order to constraint the mass of $\tilde{\chi}_1^0$. This technique will be exploited in a future analysis. However, it should be stressed, that the end-point approach, can be easily done in a favourable scenario, like the one at point B, while it could be critical if SUSY reveal itself in a scenario like the one at point G where the end-points are difficult to select or even worse in the case of point I.

It is worth noticing, that as both M($\tilde{\mathrm{b}}$) and M($\tilde{\mathrm{g}}$) depend on the $\tilde{\chi}_1^0$ mass, their difference M($\tilde{\mathrm{g}}$)-M($\tilde{\mathrm{b}}$) is on the contrary independent on M($\tilde{\chi}_1^0$). In Fig. 16 reconstructions are done shifting $\mathrm{M}(\tilde{\chi}_1^0)$ by $\pm$30 GeV/c^2. Sbottom and gluino peaks are strongly affected, while the distribution of $\mathrm{M}(\tilde{\mathrm{g}}) - \mathrm{M}(\tilde{\mathrm{b}})$ remains unchanged. Figure 17 shows the $\mathrm{M}(\tilde{\mathrm{g}}) - \mathrm{M}(\tilde{\mathrm{b}})$ peak together with the Gaussian plus polynomial fit.

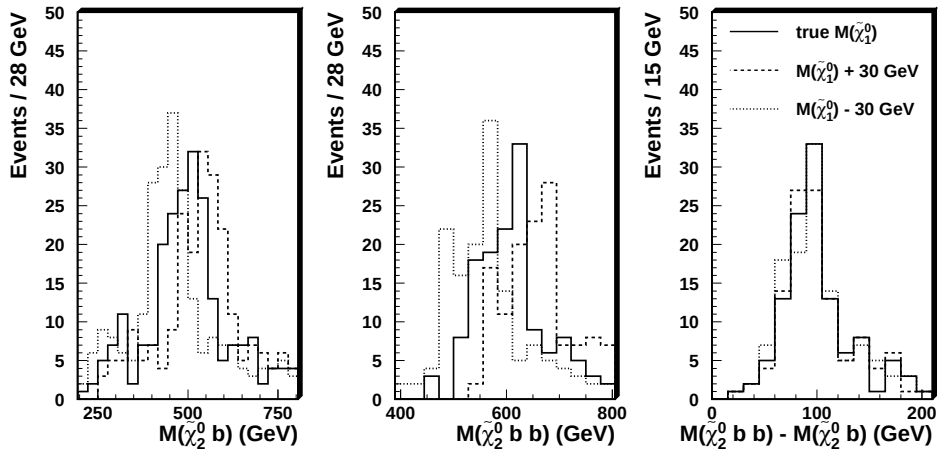

Figure 16: Sbottom mass peak (left), gluino mass peak (centre) and $\mathrm{M}(\tilde{\mathrm{g}}) - \mathrm{M}(\tilde{\mathrm{b}})$ distribution for events reconstructed assuming the true $\mathrm{M}(\tilde{\chi}_1^0)$ (black histogram), $\mathrm{M}(\tilde{\chi}_1^0) + 30$ GeV/c^2 (red histogram) and $\mathrm{M}(\tilde{\chi}_1^0) - 30$ GeV/c^2 (green histogram). The peaks are built according to the procedures described in the previous paragraphs, while for the $\mathrm{M}(\tilde{\mathrm{g}}) - \mathrm{M}(\tilde{\mathrm{b}})$ distribution the additional requirement of selecting events in the gluino peak $\pm 2.5\sigma$ is done.

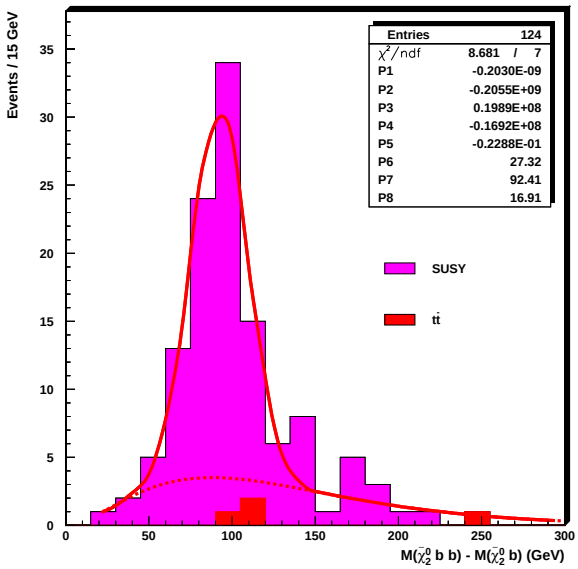

Figure 17: Result of the fit for the reconstructed $\mathrm{M}(\tilde{\mathrm{g}}) - \mathrm{M}(\tilde{\mathrm{b}})$: a Gaussian is used for the signal peak, whereas the combinatorial and Standard Model background are fitted with a polynomial. The events are selected requiring $65\ \mathrm{GeV/c^2} < \mathrm{M}_{\ell\ell} < 80\ \mathrm{GeV/c^2}$, $E_{\mathrm{T}}^{\mathrm{miss}} > 150$ GeV, $\mathrm{E}_{\mathrm{b1}} > 250$ GeV, $400\ \mathrm{GeV/c^2} < \mathrm{M}(\tilde{\chi}_2^0\mathrm{b}) < 600\ \mathrm{GeV/c^2}$ and $500\ \mathrm{GeV/c^2} < \mathrm{M}(\tilde{\chi}_2^0\mathrm{bb}) < 700\ \mathrm{GeV/c^2}$.

The measured value is

$$\mathrm{M}(\tilde{\chi}_2^0\mathrm{bb}) - \mathrm{M}(\tilde{\chi}_2^0\mathrm{b}) = 92 \pm 3\ \mathrm{GeV/c^2} \quad (26a)$$

$$\sigma[\mathrm{M}(\tilde{\chi}_2^0\mathrm{bb}) - \mathrm{M}(\tilde{\chi}_2^0\mathrm{b})] = 17 \pm 4\ \mathrm{GeV/c^2}. \quad (26b)$$

The 18% resolution achieved is rather worse than in the separate measurements of sbottom and gluino masses, but this quantity has the advantage of being totally independent from any assumption on the spectrum of undetected particles. Its measurement can hence offer a model independent information, specially important in the first months after the possible discovery of supersymmetry.

Of course, a precise $\mathrm{M}(\tilde{\chi}_1^0)$ measurement from any other analysis or, for istance, from a Linear Collider could be used as input in the present reconstruction eliminating the biggest source of systematic uncertainties. To evaluate

the dependence of sbottom, squark and gluino mass measurement on the accuracy of the $\tilde{\chi}_1^0$ mass knowledge, the reconstruction procedure has been repeated for different $\tilde{\chi}_1^0$ mass values. The dependence of M($\tilde{\mathrm{b}}$) and M($\tilde{\mathrm{g}}$) (sbottom decay chain) and of M($\tilde{\mathrm{q}}$) and M($\tilde{\mathrm{g}}$) (squark decay chain) on M($\tilde{\chi}_1^0$) is shown in Fig. 18 and in Fig. 19, respectively. All the masses of the reconstructed sparticles show a linear dependence. Performing a linear fit, we can deduce:

$$\begin{aligned}
\Delta\mathrm{M}(\tilde{\chi}_2^0\mathrm{b}) &= (1.60 \pm 0.03)\Delta M(\tilde{\chi}_1^0) \\
\Delta\mathrm{M}(\tilde{\chi}_2^0\mathrm{bb}) &= (1.62 \pm 0.05)\Delta M(\tilde{\chi}_1^0) \\
\Delta\mathrm{M}(\tilde{\chi}_2^0\mathrm{q}) &= (1.70 \pm 0.01)\Delta M(\tilde{\chi}_1^0) \\
\Delta\mathrm{M}(\tilde{\chi}_2^0\mathrm{qq}) &= (1.68 \pm 0.07)\Delta M(\tilde{\chi}_1^0)
\end{aligned}$$

In the case of the sbottom, for instance, in order to have an uncertainty less than the statistical error achieved at 300 fb^{-1}, we should have $\Delta\mathrm{M}(\tilde{\chi}_1^0) < 1.25$ GeV. This precision cannot be achieved by LHC alone, however using the combined information from LHC/LC could help us to have a deeper knowledge of the SUSY spectrum.

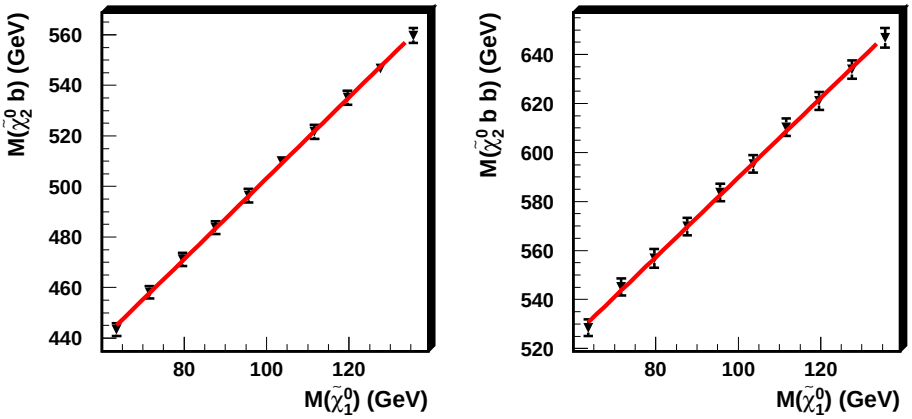

Figure 18: Dependece of sbottom and gluino masses (sbottom decay chain) vs $M(\tilde{\chi}_1^0)$.

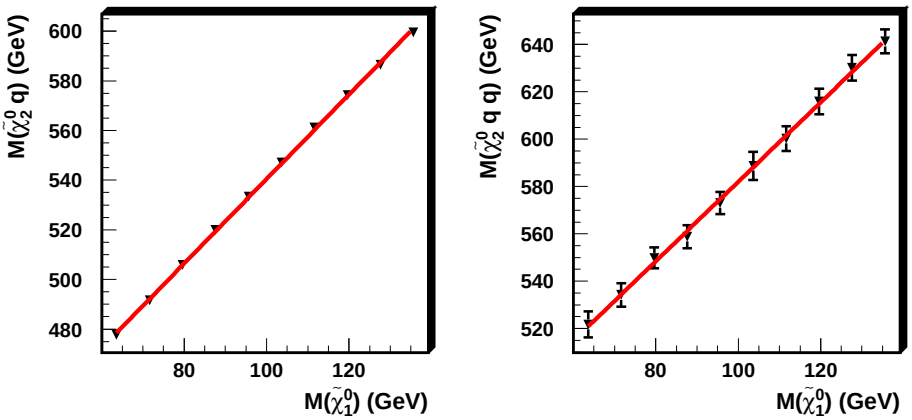

Figure 19: Dependece of squark and gluino masses (squark decay chain) vs $M(\tilde{\chi}_1^0)$.

6 Point B at high luminosity

Larger statistics can allow an optimization of cuts and a better understanding of detector and systematic effects for the reconstructions shown at Point B. Some of these effects have been studied, and a collection of optimized results has been extracted for samples corresponding to 60 fb^{-1} and 300 fb^{-1}.

6.1 Effect of the dilepton window width

The equation relating $\tilde{p}_{\tilde{\chi}_2^0}$ with $\tilde{p}_{\ell^+\ell^-}$ is less valid far from the edge. It is therefore necessary to keep the $M_{\ell\ell}$ window as narrow as possible, to avoid distortion of the peaks due to the wrong estimate of the $\tilde{\chi}_2^0$ momentum. On the other hand, it is necessary to collect a statistically significant sample to perform the reconstruction. These two opposite effects have to be opportunely tuned.

In Fig. 20, mass and width of sbottom and gluino are represented versus the lower bound on $M_{\ell\ell}$ keeping the higher bound fixed at 80 GeV/c^2. It can be seen that a too wide region yields an overestimation of the mass of both the sbottom and the gluino. The effect is more visible for the gluino. For $M_{\ell\ell}^{\rm left} > 70$ GeV/c^2, the masses reach a stable value. The widths are smaller for narrower windows: it would be important to select events as close as possible to the end-point to have a better peak resolution. This is only possible with a rich statistical sample: at point B, the quality of the peaks is highly degraded if a window in $M_{\ell\ell}$ narrower than 15 GeV/c^2 is chosen for the selection at 10 fb^{-1}, but at higher integrated luminosity tighter cuts can be used.

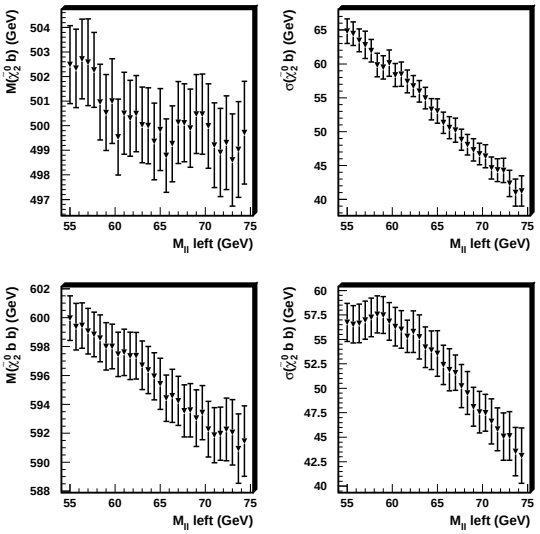

Figure 20: Sbottom and gluino masses and widths versus the lower cut on $M_{\ell\ell}$, keeping the upper cut fixed at 80 GeV/c^2.

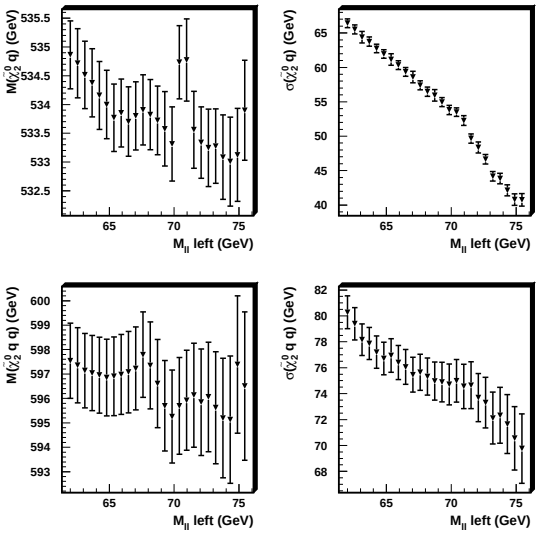

Figure 21: Squark and gluino masses and widths versus the lower cut on $M_{\ell\ell}$, keeping the upper cut fixed at 80 GeV/c^2.

A similar behaviour is observed in the squark chain, as illustrated in Fig. 21.

Figure 22 shows the mass peaks for sbottom, gluino and squark for 300 fb^{-1} of integrated luminosity, after the optimization procedures applied to the $M_{\ell\ell}$ window.

6.2 Sbottom separation

As can be seen from Fig. 22, the separation of the two sbottom contributions seems to be unaccessible even at very high luminosities due to the fact that the detector resolution is larger than the mass difference between the two sbottoms. However, with the ultimate luminosity of 300 fb^{-1}, reachable at the end of the LHC running period, it is possible to perform a double Gaussian fit on the sbottom mass distribution. In Fig. 23 the two Gaussian superimposed to the sbottom mass peak are shown. The results of the fit return $M(\tilde{b}_1) = 487 \pm 7$ GeV/c^2, $M(\tilde{b}_2) = 530 \pm 19$ GeV/c^2 in agreement with the generated value. It is worth noticing that the ratio of the coefficient of the two Gaussians, $k_1/k_2 = 2.5$, is in very good agreement with the ratio of the $\sigma \times BR$ for the two sbottom states, $\sigma \times BR(\tilde{b}_1)/\sigma \times BR(\tilde{b}_2) = 2.54$.

In Table 7 all the results obtained at point B for the three different luminosities considered are summarized. The reported errors are only statistical, as obtained by the fits. In parenthesis the reconstructed masses for $M(\tilde{\chi}_1^0) \equiv M_{\ell^+\ell^-}^{\rm max}$ are reported.

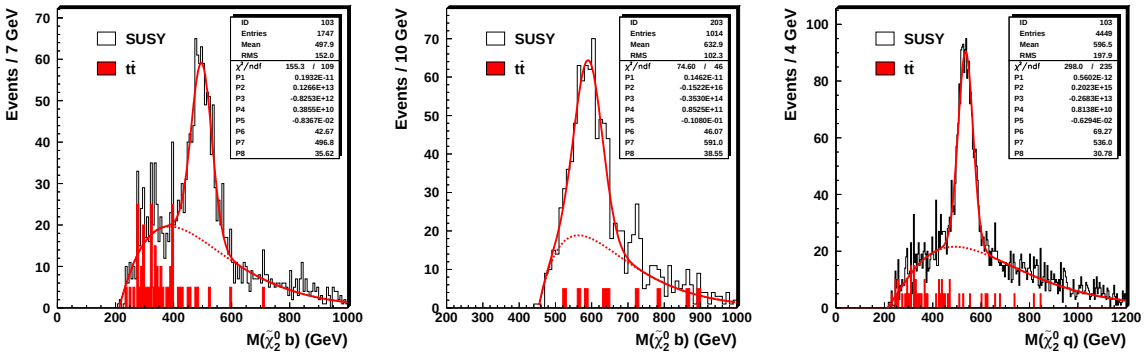

Figure 22: Invariant mass of the reconstructed sbottom (left), gluino in the sbottom chain (centre), and squark (right) for 300 fb^{-1} of integrated luminosity.

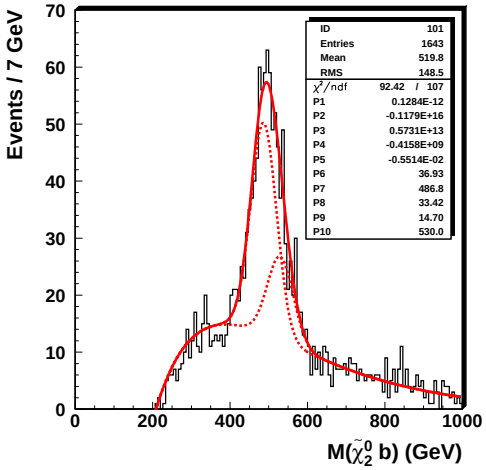

Figure 23: $M(\tilde{\chi}_2^0 b)$ mass distribution for an integrated luminosity of 300 fb^{-1}, superimposed with a double Gaussian fit.

Table 7: Sparticle mass resolutions in sbottom and squark decay chains. All the results are expressed in GeV/c^2. In parenthesis the reconstructed masses for $M(\tilde{\chi}_1^0) \equiv M_{\ell^+\ell^-}^{max}$ (Sect. 5).

	$M(\tilde{b})$	$\sigma(\tilde{b})$	$M(\tilde{g})$	$\sigma(\tilde{g})$	$M(\tilde{g})$-$M(\tilde{b})$	$\sigma(\tilde{g}$-$\tilde{b})$
10 fb^{-1}	500 ± 7	42 ± 5	594 ± 7	42 ± 7	92 ± 3	17 ± 4
	(470 ± 6)	(39 ± 4)	(555 ± 6)	(42 ± 4)		
60 fb^{-1}	502 ± 4	41 ± 4	592 ± 4	46 ± 3	88 ± 2	20 ± 2
	(473 ± 4)	(37 ± 3)	(559 ± 4)	(42 ± 4)		
300 fb^{-1}	497 ± 2	36 ± 3	591 ± 3	39 ± 3	90 ± 2	23 ± 2
	(469 ± 2)	(37 ± 2)	(557 ± 3)	(38 ± 4)		
	$M(\tilde{q})$	$\sigma(\tilde{q})$	$M(\tilde{g})$	$\sigma(\tilde{g})$	$M(\tilde{g})$-$M(\tilde{q})$	$\sigma(\tilde{g}$-$\tilde{q})$
10 fb^{-1}	535 ± 3	57 ± 3	592 ± 7	75 ± 5	57 ± 3	9 ± 3
	(502 ± 3)	(56 ± 3)	(565 ± 7)	(75 ± 6)		
60 fb^{-1}	532 ± 2	36 ± 1	595 ± 2	59 ± 2	47 ± 2	16 ± 5
	(501 ± 2)	(35 ± 2)	(560 ± 3)	(66 ± 2)		
300 fb^{-1}	536 ± 1	31 ± 1	590 ± 2	59 ± 2	44 ± 2	11 ± 2
	(506 ± 1)	(31 ± 1)	(560 ± 2)	(57 ± 2)		

7 Reconstructions at Point G

In order to evaluate the effect of $\tan\beta$ on the reconstruction method, the analysis has been repeated at point G, which is defined as:

$$\begin{aligned} m_0 &= 120\ \mathrm{GeV/c^2} \\ m_{1/2} &= 375\ \mathrm{GeV/c^2} \\ \tan\beta &= 20 \\ A_0 &= 0 \\ \mu &> 0 \end{aligned}$$

The supersymmetric spectrum as resulting from the combined running of `ISASUGRA 7.51` and `PYTHIA 6.152` has been already shown in Table 1. The gluino is still the heaviest particle, like at point B, and its decay into $\tilde{t}_2$ is not kinematically allowed, while it can decay into all the other squarks.

In Table 8, the production cross sections of SUSY pairs are summarised: the total SUSY cross section is about one order of magnitude lower than at point B; $\tilde{q}\tilde{q}$ and $\tilde{q}\tilde{g}$ are the main processes, representing the 75% of the total.

Table 8: Production cross sections for the SUSY process in proton-proton collisions at 14 TeV in the centre of mass as given by `PYTHIA 6.152` with input parameters taken from `ISASUGRA 7.51`. Here the symbol $\tilde{\chi}$ indicates charginos and neutralinos, while $\tilde{q}$ is used only for the first two generation squarks, $\tilde{u}$, $\tilde{d}$, $\tilde{c}$ and $\tilde{s}$. Sbottoms and stops are represented separately from the other squarks.

Process	σ (pb)
$\tilde{\ell}\tilde{\ell}$	0.15
$\tilde{\chi}\tilde{\chi}$	0.40
$\tilde{\chi}\tilde{g}$	0.12
$\tilde{g}\tilde{g}$	0.64
$\tilde{\chi}\tilde{q}$	0.32
$\tilde{q}\tilde{g}$	3.60
$\tilde{q}\tilde{q}$	2.55
$\tilde{q}\tilde{b}$	0.06
$\tilde{b}\tilde{b}$	0.11
$\tilde{b}\tilde{g}$	0.06
$\tilde{t}\tilde{t}$	0.24
Total	8.25

With respect to the point B, the branching ratios of the gluino into squarks and sbottoms are slightly lower, while the BR of the decay $\tilde{g} \to \tilde{t}_1 t$ is a little larger. These effects are however not dramatic. What deeply influences the capability to reconstruct the whole chain is the difference of branching ratio of the decay $\tilde{\chi}_2^0 \to \tilde{\ell}\ell$, which is the starting point of the procedure. At point G it is 2.26%, while it was 16.44% at point B. It is therefore not only more difficult to separate SUSY events from Standard Model background, due to the low total cross section, but also more difficult to observe the dilepton end point among all the other processes producing leptons, due to the lower $\tilde{\chi}_2^0 \to \tilde{\ell}\ell$ branching ratio and to higher branching ratios of competitive decays. For instance, 21.52% of $\tilde{b}_2$ decays into $\tilde{t}W$, versus 2.19% at point B; 7.83% of $\tilde{\chi}_1^{\pm}$ decays into $\tilde{\chi}_1^0 W$, while at point B this decay is not allowed; 37.32% of $\tilde{\nu}_\tau$ decays into $\tilde{\tau}_1 W$, where $\tilde{\nu}_\tau$'s are copiously produced in $\tilde{\chi}_2^0$ and $\tilde{\chi}_1^{\pm}$ decays. All these processes give W's which can produce high p_T isolated leptons; other W's have to be considered as they come from top quarks, and other leptons can arise from τ's, which can be produced in $\tilde{\chi}_2^0$ or $\tilde{\chi}_1^{\pm}$ decays; there is also a contribution from Z's, which can be produced in $\tilde{\chi}_2^0 \to \tilde{\chi}_1^0 Z$ decays or from decays of stops and staus.

In Fig. 24 the invariant mass for same flavour opposite sign isolated lepton pairs is shown for SUSY events on the top of the Standard Model background, selected according to the sbottom chain criteria (Sect. 2), for a sample corresponding to an integrated luminosity of 10 fb^{-1}. The signal statistics is very poor, and it is overwhelmed by the Standard Model background. It is not possible to apply the reconstruction procedure developed for point B at so low integrated luminosity. The same figure shows the dilepton invariant mass distribution obtained applying the squark-oriented selection criteria. The end point of the distribution is a little more visible, but the number of events close to the edge is still too low to allow the application of the reconstruction procedure. It can be concluded that the CMS detector will not be capable to operate spectroscopic studies on supersymmetric particles in the very first period of its life at intermediate $\tan\beta$ values looking at the electron and muon channel. It will be necessary to

collect higher statistics or to learn how to use $\tilde{\tau}\tau$ rich final states.

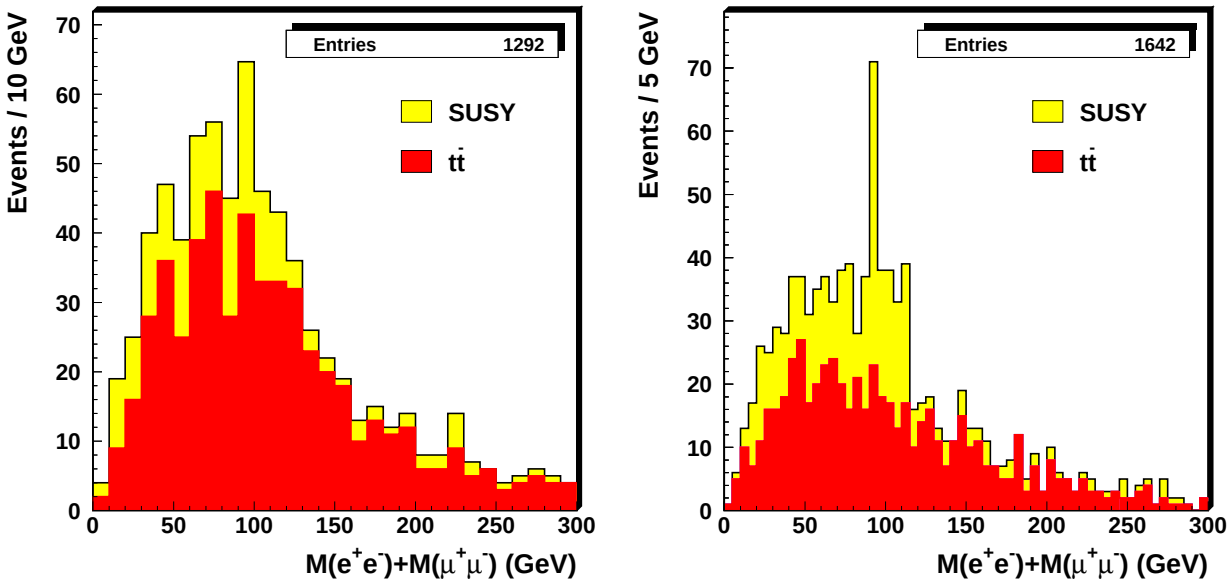

Figure 24: Left: same flavour opposite sign isolated lepton pairs for events selected according to the sbottom reconstruction method at point G, superimposed over the Standard Model background, for $E_{\mathrm{T}}^{\mathrm{miss}} > 150$ GeV. The sample correspond to an integrated luminosity of 10 fb^{-1}. Right: same for the squark chain selection.

Figure 25 shows the total dilepton invariant mass distribution for supersymmetric events together with the various contribution, with selections dedicated to sbottom chain reconstruction, for a sample corresponding to an integrated luminosity of 300 fb^{-1}. A cut on the energy of the lepton pair allows to make the $\tilde{\chi}_2^0 \to \tilde{\ell}^{\pm}\ell^{\mp} \to \tilde{\chi}_1^0\ell^{\pm}\ell^{\mp}$ visible among the other contributions, even if it is still strongly contaminated by leptons arising from W's. In Fig. 26 the SUSY dilepton distribution is plotted superimposed on the Standard Model one, for three $E_{\mathrm{T}}^{\mathrm{miss}}$ cuts. The Standard Model sample corresponds to an integrated luminosity of 60 fb^{-1}, and it is renormalized; this explains the large fluctuations in the Standard Model histograms. Due to the lower number of selected SUSY events, a very tight $E_{\mathrm{T}}^{\mathrm{miss}}$ cut is needed in order to get a good background rejection. Notwithstanding the small number of finally selected events, the edge is visible, and the reconstruction procedure can be implemented.

Again, a richer sample is selected requiring non b jets in order to reconstruct squarks or gluinos decaying into squarks. Figure 27 illustrates the dilepton invariant mass for SUSY events. In this case the $\tilde{\chi}_2^0 \to \tilde{\ell}^{\pm}\ell^{\mp} \to \tilde{\chi}_1^0\ell^{\pm}\ell^{\mp}$ decay is much more visible because it is less contaminated by W's, which in the sbottom chain are copiously produced in $\tilde{\mathrm{b}} \to \tilde{\mathrm{t}}\mathrm{W}$ decays; no decays of such kind are present in light squarks decays, and the W's contaminating the sample are produced mainly in chargino decays. A cut on $\mathrm{E}_{\ell\ell}$ makes the total distribution almost corresponding to the signal one. As in Fig. 28, a good rejection efficiency against the Standard Model background is attainable with a lower cut on the transverse missing energy with respect to the one required in the sbottom case, and the edge is clearly visible.

In both squark and sbottom chain selections, a big peak due to $\mathrm{Z} \to \ell^{\pm}\ell^{\mp}$ appears. The Z's are produced mainly in neutralino or stau decays, and can be suppressed neither by a cut on the $E_{\mathrm{T}}^{\mathrm{miss}}$ nor by the subtraction of the different flavour opposite sign lepton pairs.

Squarks and gluinos have been reconstructed following the same steps used for point B; cuts have been adjusted to take into account the jet spectra at point G. The sbottom peak is built requiring events having 100 GeV/c^2 $< \mathrm{M}_{\ell\ell} <$ 120 GeV/c^2, $E_{\mathrm{T}}^{\mathrm{miss}} > 350$ GeV and $\mathrm{E}_{\mathrm{b1}} > 350$ GeV, where E_{b1} is the energy of the leading b jets, chosen to be associated with the $\tilde{\chi}_2^0$. The mass of the $\tilde{\chi}_1^0$ is taken from the Monte Carlo. The result is shown in Fig. 29. The statistics is very poor and the performed fit is only indicative. The Standard Model background is not considered. However, less than ten Standard Model events are foreseen to be selected, versus the 89 for SUSY, and all of them should lie in the low region of the sbottom invariant mass distribution, not affecting significantly the peak.

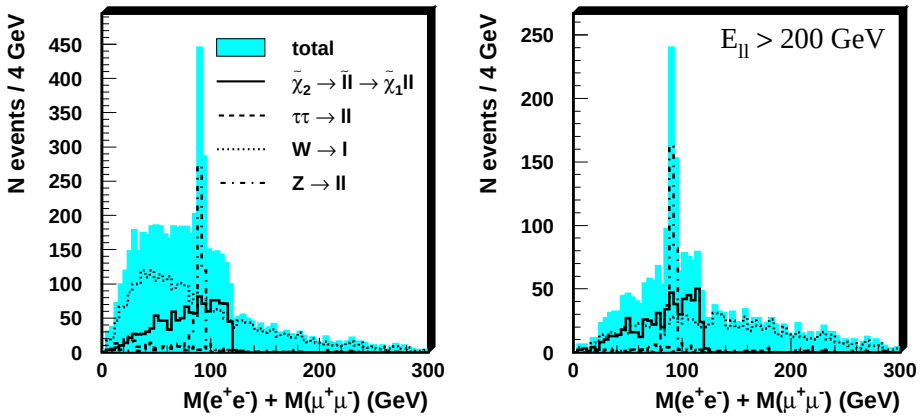

Figure 25: Invariant mass of the same flavour opposite sign isolated lepton pairs for SUSY events selected to observe the sbottom chain. On the right, the same with $E_{\ell\ell} > 200$ GeV. The integrated luminosity is 300 fb^{-1}.

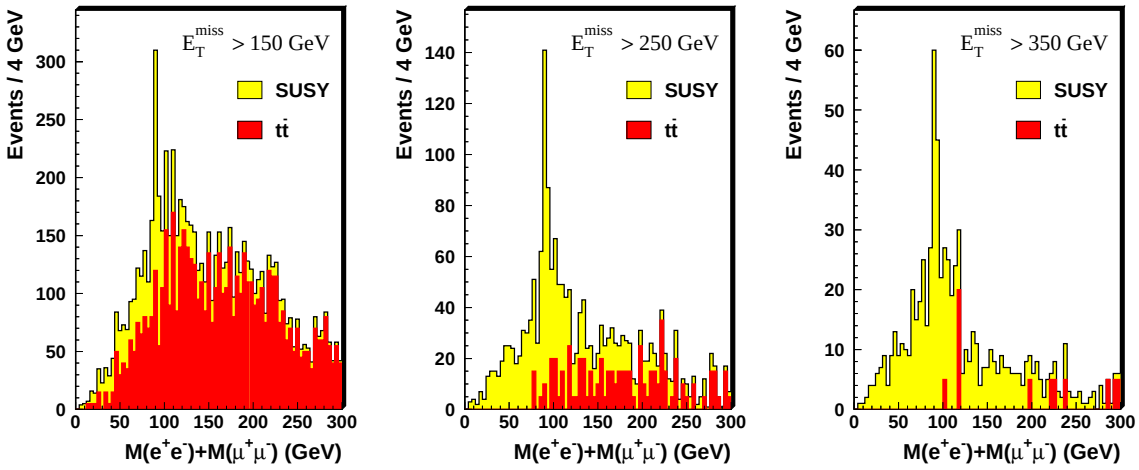

Figure 26: Invariant mass of the same flavour opposite sign isolated lepton pairs for SUSY events in the sbottom chain superimposed over the Standard Model events for $E_{\ell\ell} > 200$ GeV and for $E_T^{miss} > 150$ GeV (left), $E_T^{miss} > 250$ GeV (centre), $E_T^{miss} > 350$ GeV (right). The integrated luminosity is 300 fb^{-1}.

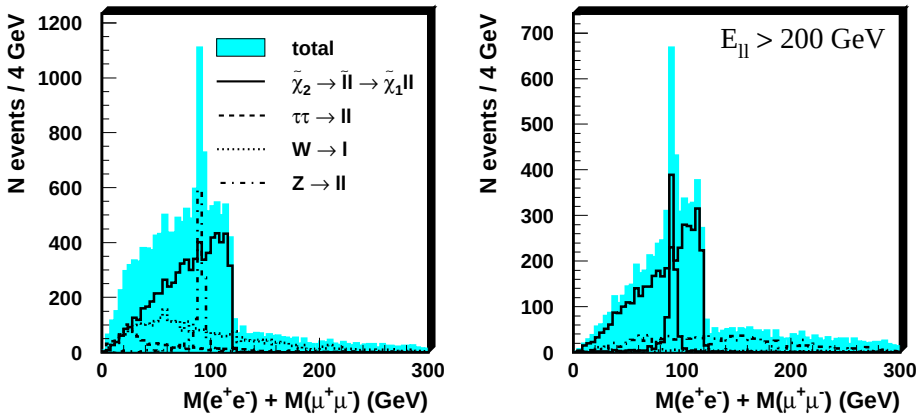

Figure 27: Invariant mass of the same flavour opposite sign isolated lepton pairs for SUSY events selected to observe the squark chain. On the right, the same with $E_{\ell\ell} > 200$ GeV. The integrated luminosity is 300 fb^{-1}.

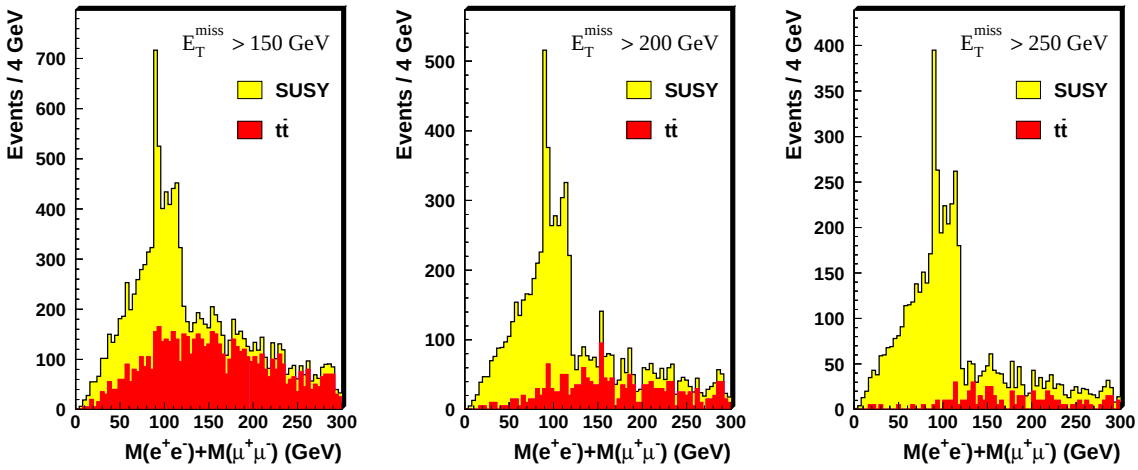

Figure 28: Invariant mass of the same flavour opposite sign isolated lepton pairs for SUSY events in the squark chain superimposed over the Standard Model events for $E_{\ell\ell} > 200$ GeV and for $E_T^{miss} > 150$ GeV (left), $E_T^{miss} > 200$ GeV (centre), $E_T^{miss} > 250$ GeV (right). The integrated luminosity is 300 fb^{-1}.

The result is

$$\mathrm{M}(\tilde{\chi}_2^0\mathrm{b}) = 720 \pm 26\ \mathrm{GeV/c^2} \quad (27a)$$
$$\sigma[\mathrm{M}(\tilde{\chi}_2^0\mathrm{b})] = 81 \pm 18\ \mathrm{GeV/c^2} \quad (27b)$$

The resolution is about 11%, quite larger than the one achieved at point B; this is caused mainly by the necessity to require a wide dilepton window to get a reasonable number of events. The statistical error is larger too. The measured mass is within the masses of the two generated sbottoms $\mathrm{M}(\tilde{\mathrm{b}}_1) = 701.9\,\mathrm{GeV/c^2}$ and $\mathrm{M}(\tilde{\mathrm{b}}_2) = 748.3\,\mathrm{GeV/c^2}$ as expected. Of course, any attempt to fit the distribution with a double Gaussian is impossible given the low statistics.

The b jet closest in angle to the reconstructed sbottom is used to build the gluino. Events are selected in the sbottom peak $\pm 2.5\sigma$: this allows to lower the cut in missing transverse energy since most of the Standard Model events are outside this region. The obtained peak is shown in Fig. 30. As for the sbottom, the fit is only indicative, and the measured quantities are affected by very large errors. However the observed gluino mass is in agreement with the generated one. The distribution of the difference between the gluino and the sbottom mass is also shown, for the same sample and with the same cuts used in the gluino peak reconstruction. The results are

$$\mathrm{M}(\tilde{\chi}_2^0\mathrm{bb}) = 852 \pm 40\ \mathrm{GeV/c^2} \quad (28a)$$
$$\sigma[\mathrm{M}(\tilde{\chi}_2^0\mathrm{bb})] = 130 \pm 43\ \mathrm{GeV/c^2} \quad (28b)$$
$$\mathrm{M}(\tilde{\chi}_2^0\mathrm{bb}) - \mathrm{M}(\tilde{\chi}_2^0\mathrm{b}) = 127 \pm 10\ \mathrm{GeV/c^2} \quad (28c)$$
$$\sigma[\mathrm{M}(\tilde{\chi}_2^0\mathrm{bb}) - \mathrm{M}(\tilde{\chi}_2^0\mathrm{b})] = 48 \pm 11\ \mathrm{GeV/c^2} \quad (28d)$$

which have to be compared with the generated values:

$$\mathrm{M}(\tilde{\mathrm{g}}) = 860.8\ \mathrm{GeV/c^2}$$
$$\mathrm{M}(\tilde{\mathrm{g}}) - \mathrm{M}(\tilde{\mathrm{b}}_1) = 158.9\ \mathrm{GeV/c^2}$$
$$\mathrm{M}(\tilde{\mathrm{g}}) - \mathrm{M}(\tilde{\mathrm{b}}_2) = 112.5\ \mathrm{GeV/c^2}$$

So, the resolution on the gluino mass is larger than 15%, and it is 38% for the mass difference.

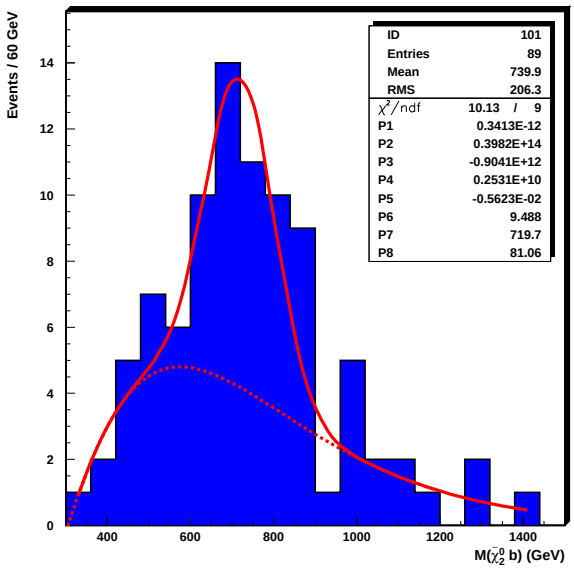

Figure 29: Invariant mass of the system $(\tilde{\chi}_2^0\mathrm{b})$ for SUSY events having $100\ \mathrm{GeV/c^2} < \mathrm{M}_{\ell\ell} < 120\ \mathrm{GeV/c^2}$, $E_{\mathrm{T}}^{\mathrm{miss}} > 350$ GeV and $\mathrm{E}_{\mathrm{b1}} > 350$ GeV at point G. The integrated luminosity is 300 fb^{-1}.

The squark mass peak (Fig. 31) has been reconstructed according to the method already described for point B, selecting events having $110\ \mathrm{GeV/c^2} < \mathrm{M}_{\ell\ell} < 120\ \mathrm{GeV/c^2}$, $E_{\mathrm{T}}^{\mathrm{miss}} > 250$ GeV and $\mathrm{E}_{\mathrm{j1}} > 300$ GeV, where E_{j1} is the hardest non b jet. The results of the fit are

$$\mathrm{M}(\tilde{\chi}_2^0\mathrm{q}) = 774 \pm 9\ \mathrm{GeV/c^2} \quad (29a)$$
$$\sigma[\mathrm{M}(\tilde{\chi}_2^0\mathrm{q})] = 84 \pm 9\ \mathrm{GeV/c^2} \quad (29b)$$

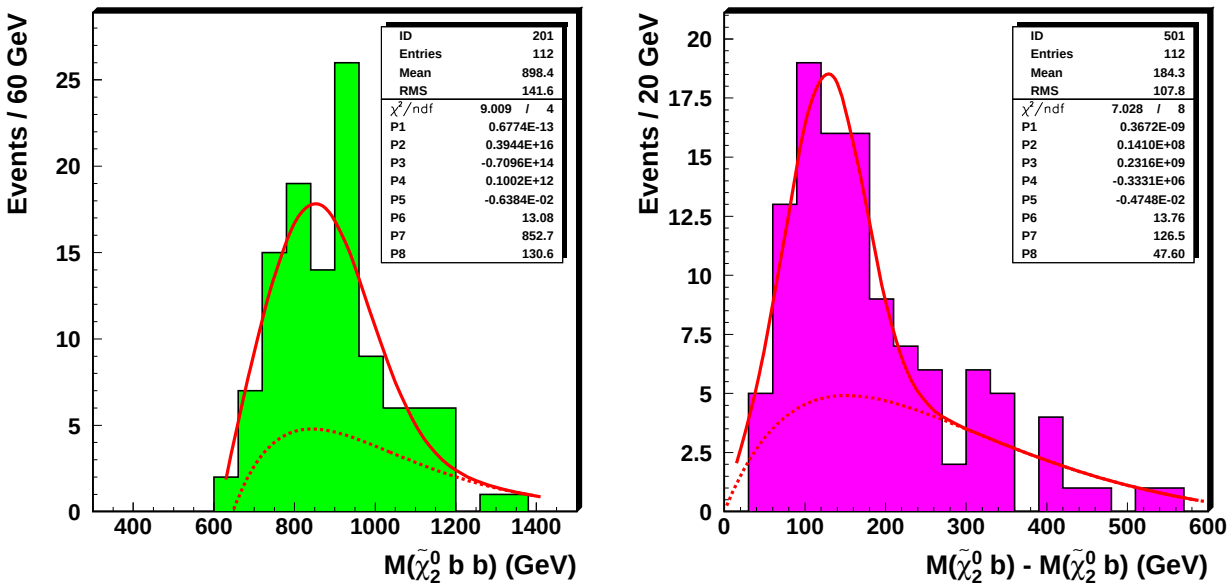

Figure 30: Left: invariant mass of the system $(\tilde{\chi}_2^0 \mathrm{bb})$ for SUSY events having 100 GeV/c^2< $\mathrm{M}_{\ell\ell}$ < 120 GeV/c^2, $E_{\mathrm{T}}^{\mathrm{miss}} > 200$ GeV and $\mathrm{E}_{\mathrm{b1}} > 350$ GeV and 560 GeV/c^2 < $\mathrm{M}(\tilde{\chi}_2^0 \mathrm{b})$ < 880 GeV/c^2, at point G. Right: distribution of $\mathrm{M}(\tilde{\chi}_2^0 \mathrm{bb}) - \mathrm{M}(\tilde{\chi}_2^0 \mathrm{b})$, with the same cuts. Both plots refer to an integrated luminosity of 300 fb^{-1}.

The measured mass agrees with the generated masses of light squark left components: $\mathrm{M}(\tilde{\mathrm{u}}_{\mathrm{L}}) = \mathrm{M}(\tilde{\mathrm{c}}_{\mathrm{L}}) = 773.88$ GeV/c^2, $\mathrm{M}(\tilde{\mathrm{d}}_{\mathrm{L}}) = \mathrm{M}(\tilde{\mathrm{s}}_{\mathrm{L}}) = 778.02$ GeV/c^2. The contribution from the right components is negligible since $\mathrm{BR}(\tilde{\mathrm{q}}_{\mathrm{R}} \to \tilde{\chi}_2^0 \mathrm{q}) = 0.27\%$. The 11% resolution is of the same order of the sbottom one, but the statistical error is much smaller.

Figure 32 shows the gluino reconstructed in the squark chain, with events having 110 GeV/c^2< $\mathrm{M}_{\ell\ell}$ < 120 GeV/c^2, $E_{\mathrm{T}}^{\mathrm{miss}} > 250$ GeV, $\mathrm{E}_{\mathrm{j1}} > 300$ GeV, 575 GeV/c^2 < $\mathrm{M}(\tilde{\chi}_2^0 \mathrm{q})$ < 975 GeV/c^2, and $\mathrm{E}_{\mathrm{j2}} < 150$ GeV, where E_{j2} is the energy of the second selected jet. The result is

$$\mathrm{M}(\tilde{\chi}_2^0 \mathrm{qq}) = 853 \pm 11 \text{ GeV/c}^2 \quad (30a)$$

$$\sigma[\mathrm{M}(\tilde{\chi}_2^0 \mathrm{qq})] = 126 \pm 11 \text{ GeV/c}^2 \quad (30b)$$

It can be concluded that point G is a boundary point for sparticle reconstruction in the electron and muon channel: at high integrated luminosity, some information about the sparticle mass spectrum can be extracted, but the measurements are affected by large errors, and they can be considered only as rough estimate. This is mainly caused by the small branching ratio of the $\tilde{\chi}_2^0$ decays into electrons and muons.

8 Point I

The five mSUGRA parameters defining the benchmark point I are

$$\begin{aligned} m_0 &= 180 \quad \text{GeV/c}^2 \\ m_{1/2} &= 350 \quad \text{GeV/c}^2 \\ \tan\beta &= 35 \\ A_0 &= 0 \\ \mu &> 0 \end{aligned}$$

so it is not far from point G, with the main difference in $\tan\beta$.

Since m_0 and $m_{1/2}$ are quite close to point G, the spectrum is not very different. The $\tan\beta$ parameter influences nevertheless the $\tilde{\chi}_2^0$ decay branching ratios: only 0.25% of them decay now into electrons and muons, and more

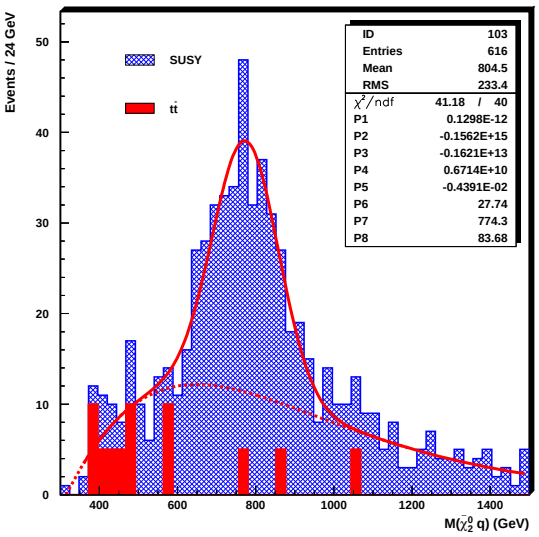

Figure 31: Invariant mass of the system $(\tilde{\chi}_2^0 \mathrm{q})$ for SUSY events having 110 GeV/c^2< $\mathrm{M}_{\ell\ell}$ < 120 GeV/c^2, $E_{\mathrm{T}}^{\mathrm{miss}} > 250$ GeV and $\mathrm{E}_{\mathrm{b1}} > 350$ GeV at point G. The integrated luminosity is 300 fb^{-1}.

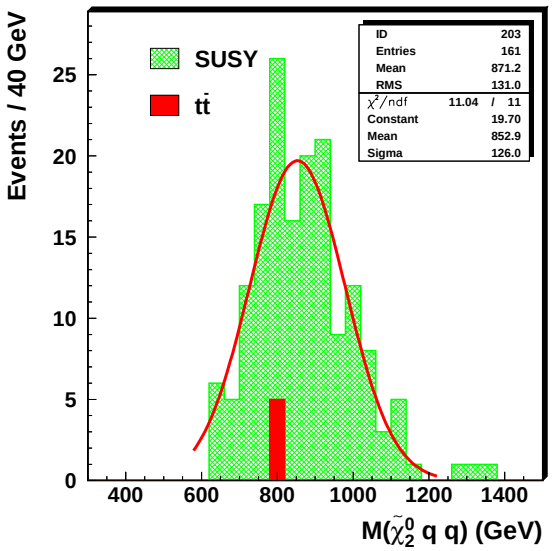

Figure 32: Invariant mass of the system $(\tilde{\chi}_2^0 \mathrm{qq})$ for SUSY events having 110 GeV/c^2< $\mathrm{M}_{\ell\ell}$ < 120 GeV/c^2, $E_{\mathrm{T}}^{\mathrm{miss}} > 250$ GeV, $\mathrm{E}_{\mathrm{j1}} > 300$ GeV, $\mathrm{E}_{\mathrm{j1}} > 150$ GeV and 575 GeV/c^2 < $\mathrm{M}(\tilde{\chi}_2^0 \mathrm{q})$ < 975 GeV/c^2, at point G

than 98% into taus. Figure 33 shows the invariant mass distribution of same flavour opposite sign lepton pairs at point I for a sample corresponding to an integrated luminosity of 300 fb^{-1}, for the sbottom and squark selection methods illustrated in the previous sections. In both plots the solid lines, representing the contribution from $\tilde{\chi}_2^0 \to \tilde{\ell}^{\pm}\ell^{\mp} \to \tilde{\chi}_1^0 \ell^{\pm}\ell^{\mp}$, which is the starting point of the procedure, are completely overwhelmed by the other curves representing other lepton sources, and no clear end-point can be identified. In addition, the end-point of the distribution falls very close to the Z region: even if cuts can be tried to reduce fake leptons from W's, irreducible background arising from Z doesn't allow the observation of the dilepton edge.

This benchmark point is an example of a supersymmetric scenario for which the methods presented above cannot be applied to reconstruct squark and gluino mass peaks. It could be useful to perform other studies exploiting other decays to evaluate the CMS capability to observe sparticles peaks. For example, the rising of $\tilde{\chi}_2^0 \to \tilde{\tau}^{\pm}\tau^{\mp} \to \tilde{\chi}_1^0 \tau^{\pm}\tau^{\mp}$ branching ratio at increasing $\tan\beta$ can result in a channel complementary to the one just presented.

Acknowledgements

We would like to thank D. Denegri for his guidance and for reading the manuscript. We are also grateful to A. De Roeck and F. Moortgat for helpful discussions.

References

[1] **CMS Note 1998/006**, D. Denegri at al., *Discovery potential for Supersymmetry in CMS*.

[2] M. Battaglia *et al.*, *Proposed Post-LEP Benchmarks for Supersymmetry*, Eur. Phys. J. **C22** (2001) 535, hep-ph/0106204, CERN-TH/2001-150.

[3] H. Baer, F. E. Paige, S. D. Protopopescu and X. Tata, *ISAJET 7.48: A Monte Carlo event generator for* pp, $\bar{\mathrm{p}}$p, *and* $\mathrm{e}^+\mathrm{e}^-$ *reactions*, hep-ph/0001086.

[4] T. S̈jostrand *et al.*, Comput. Phys. Commun. 82 (1994) 74;
T. S̈jostrand *et al.*, Comput. Phys. Commun. 135 (2001) 238.

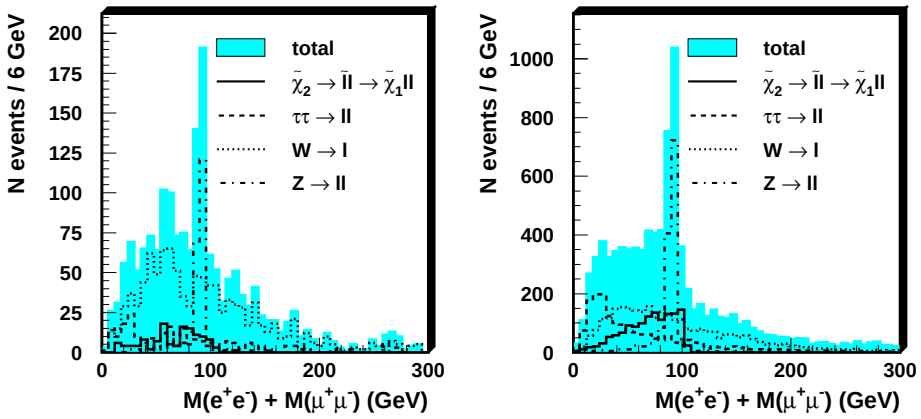

Figure 33: Invariant mass of the same flavour opposite sign isolated lepton pairs for SUSY events at point I, for events selected according to the sbottom chain reconstruction method (left) and to the squark chain one (right). The integrated luminosity is 300 fb^{-1}.

[5] S. Abdullin, A. Khanov, N. Stepanov, *CMSJET*, CMS TN/94-180.

[6] M. Chiorboli, *Supersymmetric Particle Reconstructions with the CMS detector at LHC*, Ph.D. Thesis, http://cmsdoc.cern.ch/documents/03/doc2003_002.pdf.

[7] I. Iashvili, A. Kharchilava, *Search for the Next-to-Lightest Neutralino*, CMS Note 1997/065, hep-ph/9712393; D. Denegri, W. Majerotto, L. Rurua, *Constraining the minimal supergravity model parameter* $\tan\beta$ *by measuring the dilepton mass distribution at LHC*, Phys. Rev. **D60** (1999) 035008.

[8] H. Baer, C.H. Chen, F. Paige, X. Tata, Phys. Rev. **D50** (1994) 4508.

[9] V. Drollinger, V. Karimäki, S. Lehti, N. Stepanov, A. Khanov, *Upgrade of Fast Tracker Response Simulation, the FATSIM utility*, CMS IN 2000/034, 2000.

[10] ATLAS Collaboration, *Detector and Physics Performance TDR*,CERN/LHCC 99-14.

[11] I. Hinchliffe *et al.*, *Precision SUSY measurements at LHC: Point 3.*, ATLAS Internal Note, 1997, ATLAS-NOTE-Phys-109; F. Gianotti, *Precision SUSY measurements with ATLAS for SUGRA Point 4*, ATLAS Internal Note, 1997, PHYS-No-110; G. Polesello *et al., Precision SUSY measurements with ATLAS fro SUGRA point 5*, ATLAS Internal Note, 1997, PHYS-No-111.